



HAL
open science

Diagenetic History and Biosignature Preservation Potential of Fine-Grained Rocks at Hogwallow Flats, Jezero Crater, Mars

A. Broz, B. Horgan, H. Kalucha, J. Johnson, C. Royer, E. Dehouck, L. Mandon, E. Cardarelli, B. Garczynski, J. Haber, et al.

► **To cite this version:**

A. Broz, B. Horgan, H. Kalucha, J. Johnson, C. Royer, et al.. Diagenetic History and Biosignature Preservation Potential of Fine-Grained Rocks at Hogwallow Flats, Jezero Crater, Mars. *Journal of Geophysical Research. Planets*, 2024, 129 (11), 10.1029/2024JE008520 . hal-04805795

HAL Id: hal-04805795

<https://hal.science/hal-04805795v1>

Submitted on 28 Nov 2024

HAL is a multi-disciplinary open access archive for the deposit and dissemination of scientific research documents, whether they are published or not. The documents may come from teaching and research institutions in France or abroad, or from public or private research centers.

L'archive ouverte pluridisciplinaire **HAL**, est destinée au dépôt et à la diffusion de documents scientifiques de niveau recherche, publiés ou non, émanant des établissements d'enseignement et de recherche français ou étrangers, des laboratoires publics ou privés.



Distributed under a Creative Commons Attribution 4.0 International License

Special Collection:

The Perseverance Rover's
Exploration of the Western Fan
Front, Jezero Crater, Mars

Key Points:

- Fine-grained clastic sedimentary rocks at the Hogwallow Flats member underwent limited diagenesis
- Diagenesis may have occurred in a lake or a shallow river plain and later when the sediments were shallowly buried
- Mottling features, sulfates and clay minerals within drilled rock core samples for Mars Sample Return have high astrobiological potential

Supporting Information:

Supporting Information may be found in the online version of this article.

Correspondence to:

A. P. Broz,
abroz@purdue.edu

Citation:

Broz, A. P., Horgan, B., Kalucha, H., Johnson, J. R., Royer, C., Dehouck, E., et al. (2024). Diagenetic history and biosignature preservation potential of fine-grained rocks at Hogwallow Flats, Jezero crater, Mars. *Journal of Geophysical Research: Planets*, 129, e2024JE008520. <https://doi.org/10.1029/2024JE008520>

Received 14 JUN 2024

Accepted 9 OCT 2024

Author Contributions:

Conceptualization: A. P. Broz, B. Horgan, H. Kalucha, L. Mandon, E. L. Cardarelli, B. Garczynski, J. H. Haber, K. C. Benison, N. Mangold, T. Bosak, J. I. Simon, P. Gasda, E. Clave, B. S. Kathir, M. Zawaski, S. Siljeström, N. Randazzo, L. Kah, W. Rapin, A. J. Williams, J. I. Núñez, J. F. Bell, R. C. Wiens
Data curation: A. P. Broz, B. Horgan
Formal analysis: A. P. Broz, B. Horgan, H. Kalucha, E. Dehouck, L. Mandon,

© 2024. The Author(s).

This is an open access article under the terms of the [Creative Commons Attribution License](https://creativecommons.org/licenses/by/4.0/), which permits use, distribution and reproduction in any medium, provided the original work is properly cited.

Diagenetic History and Biosignature Preservation Potential of Fine-Grained Rocks at Hogwallow Flats, Jezero Crater, Mars

A. P. Broz^{1,2} , B. Horgan¹ , H. Kalucha³ , J. R. Johnson⁴ , C. Royer¹, E. Dehouck⁵ , L. Mandon³, E. L. Cardarelli^{6,7} , B. Garczynski⁸ , J. H. Haber⁹ , K. C. Benison¹⁰ , E. Ives⁶ , K. M. Stack⁶, N. Mangold¹¹ , T. Bosak¹² , J. I. Simon¹³ , P. Gasda¹⁴ , E. Clave¹⁵, B. S. Kathir⁸ , M. Zawaski¹⁶ , R. Barnes¹⁷ , S. Siljeström¹⁸, N. Randazzo¹⁹, J. M. Madariaga²⁰ , K. Farley^{3,6}, J. Maki⁶ , L. Kah²¹ , W. Rapin²², L. L. Kivrak²³, A. J. Williams²³ , E. Hausrath²⁴ , J. I. Núñez⁴ , F. Gómez²⁵ , A. Steele²⁶ , T. Fouchet²⁷ , J. F. Bell²⁸, and R. C. Wiens¹ 

¹Purdue University, West Lafayette, IN, USA, ²University of Oregon, Eugene, OR, USA, ³California Institute of Technology, Pasadena, CA, USA, ⁴Johns Hopkins University Applied Physics Laboratory, Laurel, MD, USA, ⁵LGL-TPE, UMR 5276, CNRS, ENSL, UJM, Université Claude Bernard Lyon 1, Villeurbanne, France, ⁶Jet Propulsion Laboratory, California Institute of Technology, Pasadena, CA, USA, ⁷University of California, Los Angeles, Los Angeles, CA, USA, ⁸Western Washington University, Bellingham, WA, USA, ⁹Smithsonian Institution, Washington, DC, USA, ¹⁰West Virginia University, Morgantown, WV, USA, ¹¹LPG, CNRS, UMR612, Nantes Université, Université Angers, Nantes, France, ¹²Massachusetts Institute of Technology, Cambridge, MA, USA, ¹³NASA Johnson Space Center, Houston, TX, USA, ¹⁴Los Alamos National Laboratory, Los Alamos, NM, USA, ¹⁵University of Bordeaux, Bordeaux, France, ¹⁶Texas A&M University, College Station, TX, USA, ¹⁷Imperial College London, London, Austria, ¹⁸RISE Research Institutes of Sweden, Stockholm, Sweden, ¹⁹University of Alberta, Edmonton, AB, Canada, ²⁰University of the Basque Country, Leioa, Spain, ²¹University of Tennessee, Knoxville, TN, USA, ²²Institut de Recherche en Astrophysique et Planétologie, Toulouse, France, ²³University of Florida, Gainesville, FL, USA, ²⁴University of Nevada, Las Vegas, Las Vegas, NV, USA, ²⁵Centro de Astrobiología (INTA-CSIC), Madrid, Spain, ²⁶Carnegie Institution for Science, Washington, DC, USA, ²⁷Observatoire de Paris, CNRS, Université PSL, Sorbonne Université, Université Paris Cité, Paris, France, ²⁸Arizona State University, Tempe, AZ, USA

Abstract The Mars 2020 *Perseverance* rover discovered fine-grained clastic sedimentary rocks in the “Hogwallow Flats” member of the “Shenandoah” formation at Jezero crater, Mars. The Hogwallow Flats member shows evidence of multiple phases of diagenesis including Fe/Mg-sulfate-rich (20–30 wt. %) outcrop transitioning downward into red-purple-gray mottled outcrop, Fe/Mg clay minerals and oxides, putative concretions, occasional Ca sulfate-filled fractures, and variable redox state over small (cm) spatial scales. This work uses Mastcam-Z and SuperCam instrument data to characterize and interpret the sedimentary facies, mineralogy and diagenetic features of the Hogwallow Flats member. The lateral continuity of bedrock similar in tone and morphology to Hogwallow Flats that occurs over several km within the western Jezero sedimentary fan suggests widespread deposition in a lacustrine or alluvial floodplain setting. Following deposition, sediments interacted with multiple fluids of variable redox state and salinity under habitable conditions. Three drilled sample cores were collected from this interval of the Shenandoah formation as part of the Mars Sample Return campaign. These samples have very high potential to preserve organic compounds and biosignatures. Drill cores may partially include dark-toned mottled outcrop that lies directly below light-toned, sulfate-cemented outcrop. This facies may represent some of the least oxidized material observed at this interval of the Shenandoah formation. This work reconstructs the diagenetic history of the Hogwallow Flats member and discusses implications for biosignature preservation in rock samples for possible return to Earth.

Plain Language Summary The Mars 2020 *Perseverance* rover discovered sedimentary rocks in Jezero crater during the second year of its mission. Some of these rocks were informally named the “Hogwallow Flats” member of the “Shenandoah” formation. These rocks contain abundant clay minerals and sulfates, indicating ancient interactions with liquid water. They may preserve organic matter and signs of life that could tell us whether life was ever present in Jezero crater billions of years ago. The sediments here appear to have undergone physical and chemical changes after deposition—called diagenesis—when interacting with liquid water. These changes, which may have occurred in a lake or a shallow river plain and later when the sediments were shallowly buried, are often associated with favorable conditions for preserving signs of ancient life.

E. L. Cardarelli, B. Garczynski,
K. C. Benison, N. Mangold, T. Bosak,
J. I. Simon, P. Gasda, E. Clave,
B. S. Kathir, M. Zawaski, R. Barnes,
S. Siljeström, J. M. Madariaga, J. Maki,
A. J. Williams, E. Hausrath, J. F. Bell,
R. C. Wiens

Funding acquisition: K. M. Stack,
T. Bosak, K. Farley, T. Fouchet, J. F. Bell,
R. C. Wiens

Investigation: A. P. Broz, B. Horgan,
H. Kalucha, E. Dehouck, L. Mandon,
E. L. Cardarelli, B. Garczynski,
J. H. Haber, K. C. Benison, E. Ives,
N. Mangold, T. Bosak, J. I. Simon,
P. Gasda, E. Clave, B. S. Kathir,
M. Zawaski, R. Barnes, S. Siljeström,
L. Kah, A. J. Williams, E. Hausrath,
F. Gómez, J. F. Bell, R. C. Wiens

Methodology: A. P. Broz, B. Horgan,
H. Kalucha, L. Mandon, E. L. Cardarelli,
B. Garczynski, J. H. Haber, K. C. Benison,
N. Mangold, T. Bosak, J. I. Simon,
B. S. Kathir, R. Barnes, S. Siljeström,
N. Randazzo, J. M. Madariaga, L. Kah,
A. J. Williams, J. I. Núñez, J. F. Bell,
R. C. Wiens

Project administration: K. M. Stack,
K. Farley, J. Maki, T. Fouchet, J. F. Bell

Resources: A. P. Broz, B. Horgan,
L. Mandon, E. L. Cardarelli,
B. Garczynski, N. Mangold, J. I. Simon,
P. Gasda, M. Zawaski, R. Barnes,
S. Siljeström, J. Maki, L. Kah, W. Rapin,
A. J. Williams, J. F. Bell, R. C. Wiens

Software: R. Barnes, L. Kah, J. F. Bell,
R. C. Wiens

Supervision: B. Horgan, E. Dehouck,
K. M. Stack, N. Mangold, T. Bosak,
J. I. Simon, K. Farley, L. Kah, T. Fouchet,
J. F. Bell, R. C. Wiens

Validation: B. Horgan, E. Dehouck,
L. Mandon, E. L. Cardarelli,
B. Garczynski, J. H. Haber, K. C. Benison,
E. Ives, N. Mangold, T. Bosak, J. I. Simon,
P. Gasda, E. Clave, S. Siljeström,
J. M. Madariaga, L. Kah, W. Rapin,
A. J. Williams, J. I. Núñez, A. Steele,
R. C. Wiens

Visualization: A. P. Broz, E. L. Cardarelli,
B. Garczynski, J. H. Haber, N. Randazzo,
J. Maki, J. F. Bell, R. C. Wiens

Writing – original draft: A. P. Broz,
B. Horgan

Writing – review & editing: B. Horgan,
H. Kalucha, E. Dehouck, L. Mandon,
E. L. Cardarelli, B. Garczynski,
J. H. Haber, K. C. Benison, E. Ives,
N. Mangold, T. Bosak, J. I. Simon,
P. Gasda, E. Clave, B. S. Kathir,
M. Zawaski, R. Barnes, S. Siljeström,
J. M. Madariaga, A. J. Williams,
E. Hausrath, R. C. Wiens

However, these changes may also have resulted in the breakdown of these signs of life. This work reconstructs the geologic history of the Hogwallow Flats member and discusses the importance of these rocks for the search for ancient life on Mars. A total of three rock cores were collected by *Perseverance* from these rocks for return to Earth. These samples have very high potential to preserve organic matter and signs of ancient life.

1. Introduction

The Mars 2020 *Perseverance* rover landed on 18 February 2021 in Jezero crater, Mars and has been exploring sedimentary and igneous rocks associated with an ancient sedimentary fan within the crater (Figure 1). The crater itself is inferred to have formed between 3.8 and 4 Ga (Mandon et al., 2020) and later hosted a lake and delta system that was active in the late Noachian and/or early Hesperian (3.6–3.8 billion years ago) (Mangold et al., 2021). The preserved sedimentary fan deposits within the crater are evidence of an active hydrological regime during that time (Fassett & Head, 2005; Goudge et al., 2018; Mangold et al., 2021). The primary objectives of the Mars 2020 mission are to (a) constrain the geologic processes that formed and modified the rocks of Jezero crater, and (b) to search for habitable environments and biosignatures (Farley et al., 2020). *Perseverance* also has an objective to collect rock and regolith samples that could be returned to Earth by the mid-2030s as part of the Mars Sample Return (MSR) campaign (Beatty et al., 2019; Meyer et al., 2022).

After completing exploration of aqueously altered igneous rocks on the Jezero crater floor (Farley et al., 2022; Sun et al., 2023; Wiens et al., 2022), on Sol ~416 (April 2022) *Perseverance* arrived at a sequence of sedimentary rocks exposed along the eastern edge of the western Jezero fan (Figure 1). This sedimentary succession, informally known as the “Shenandoah formation” (all names used here are informal), is approximately 25 m thick and composed of a suite of sedimentary rocks (Stack et al., 2024) that overlie the Crater Floor igneous units, informally known as the Seitah and Maaz formations (Farley et al., 2022; Paige et al., 2024). Sediments of the Shenandoah formation were likely deposited in a range of depositional environments, including alluvial plain, lacustrine, and deltaic settings (Stack et al., 2024). Several key questions emerge from the exploration of rocks in Jezero crater and motivate the present work: Did the deposition and diagenesis of these sediments occur under habitable conditions? Are diagenetic features and textures similar to those observed elsewhere on Mars? Is the diagenetic history of these rocks conducive for the preservation of biosignatures over geological time scales?

The focus of this paper is on the unique, fine-grained rocks of the “Hogwallow Flats” and “Yori Pass” members of the Shenandoah formation. The sedimentology and stratigraphic context of these intervals can be found in other recent publications (Benison et al., 2024; Stack et al., 2024). These rocks show evidence of diagenesis, including Fe/Mg sulfate-rich (20–30 wt. %) bedrock transitioning downward to red-green-gray mottled bedrock (Broz et al., 2024), as well as Fe/Mg clay minerals, oxides, putative concretions (Kalucha et al., 2024), Ca sulfate-filled fractures (Benison et al., 2024; Nachon et al., 2023), and dark-toned rock coatings (Lanza et al., 2023).

2. Perseverance’s Investigation of the Hogwallow Flats Member

Perseverance explored the Hogwallow Flats member at Hawksbill Gap from mission Sols ~470–520 (Figure 1). After exploration of lower Shenandoah formation strata including the Hughes River Gap and Devil’s Tanyard members, *Perseverance* encountered on Sol 470 the “Wildcat Ridge” outcrop of the Hogwallow Flats member, which was a light-toned, fractured mudstone that was underlain by thinly laminated, recessive and dark-toned mudstone (Figure 2) (grain size designations by Stack et al., 2024). The outcrop extends approximately 200 m along strike and is intermittently buried by aeolian bedforms. It appears to be roughly sub-horizontal with estimated dip angles ranging from ~5 to 8° to the southeast (Barnes et al., 2023). Outcrop exhibiting these characteristics can be traced laterally for over 500 m (Stack et al., 2024).

The Hogwallow Flats member of the Shenandoah formation consists of: (a) a basal red-green-gray mottled mudstone with lenses of deformed/contorted laminations that transitions into a laminated, sulfate-bearing mudstone/sandstone, (b) a middle interval of platy, low-angle cross stratified sandstone overlain by, (c) tan to purple-hued mudstone with deformed/contorted laminations (Stack et al., 2024). Previous grain size designations by Stack et al. (2024) indicated a mudstone. The total thickness is approximately 3 m.

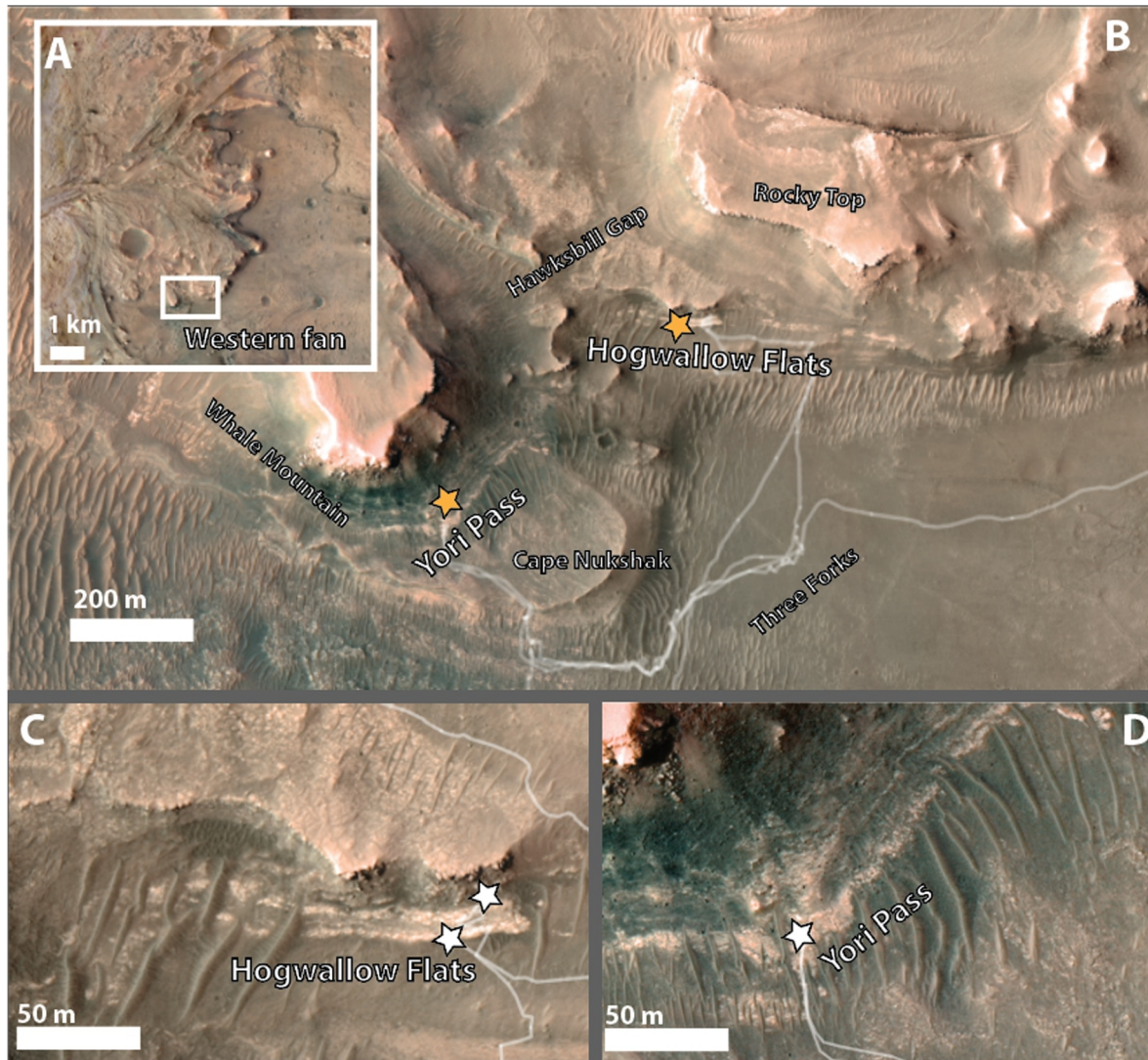


Figure 1. Orbital context of the Hogwallow Flats and Yori Pass members in the western Jezero fan front region. (a) HiRISE image of western Jezero fan (Ferguson et al., 2020) (77.387, 18.499); (b) Zoom on fan front region showing locations of Hogwallow Flats (Hawkswill Gap) and Yori Pass (Cape Nukshak) (orange stars) where white trace indicates rover traverse; (c) and (d) Zoom of light-toned layers at Hogwallow Flats (Wildcat Ridge outcrop) (77.4055481, 18.4589106) and Yori Pass (Hidden Harbor outcrop) (77.39915639, 18.45367453) showing locations where drilled samples were collected (white stars).

At Cape Nukshak (Figure 1), *Perseverance* explored a possible lateral equivalent of the Hogwallow Flats member, informally named the “Yori Pass” member, beginning around Sol 600. Here, a light-toned outcrop known as “Hidden Harbor” revealed textural, morphological and geochemical similarities to the Hogwallow Flats member (Stack et al., 2024), although intermittent cover by aeolian bedforms prevented continuous tracing of exposed bedrock between the Hogwallow Flats member and the Yori Pass member (Figure 3). The Yori Pass member is composed of sulfate-bearing, recessively weathered and laminated mudstone and sandstone that transitions upwards into a cross-stratified coarse sandstone (Stack et al., 2024). The total thickness of the Yori Pass member is approximately 10 m. The uppermost interval contains approximately 3 m of coarse-grained laminated and cross-stratified sandstone that sharply transition downward into approximately 0.5 m of thinly laminated, deformed, mottled and recessively weathered mudstone (with inferred grain size). This stratigraphy was particularly well-exposed at the Intricate Bay outcrop, a long-distance Mastcam-Z target acquired while at the Hidden Harbor outcrop (Figure 3b). Based on lithological similarities and lateral continuity observed from orbit, we interpret the Yori Pass member to be a lateral continuation of the Hogwallow Flats member (Figure S2 in Supporting Information S1).

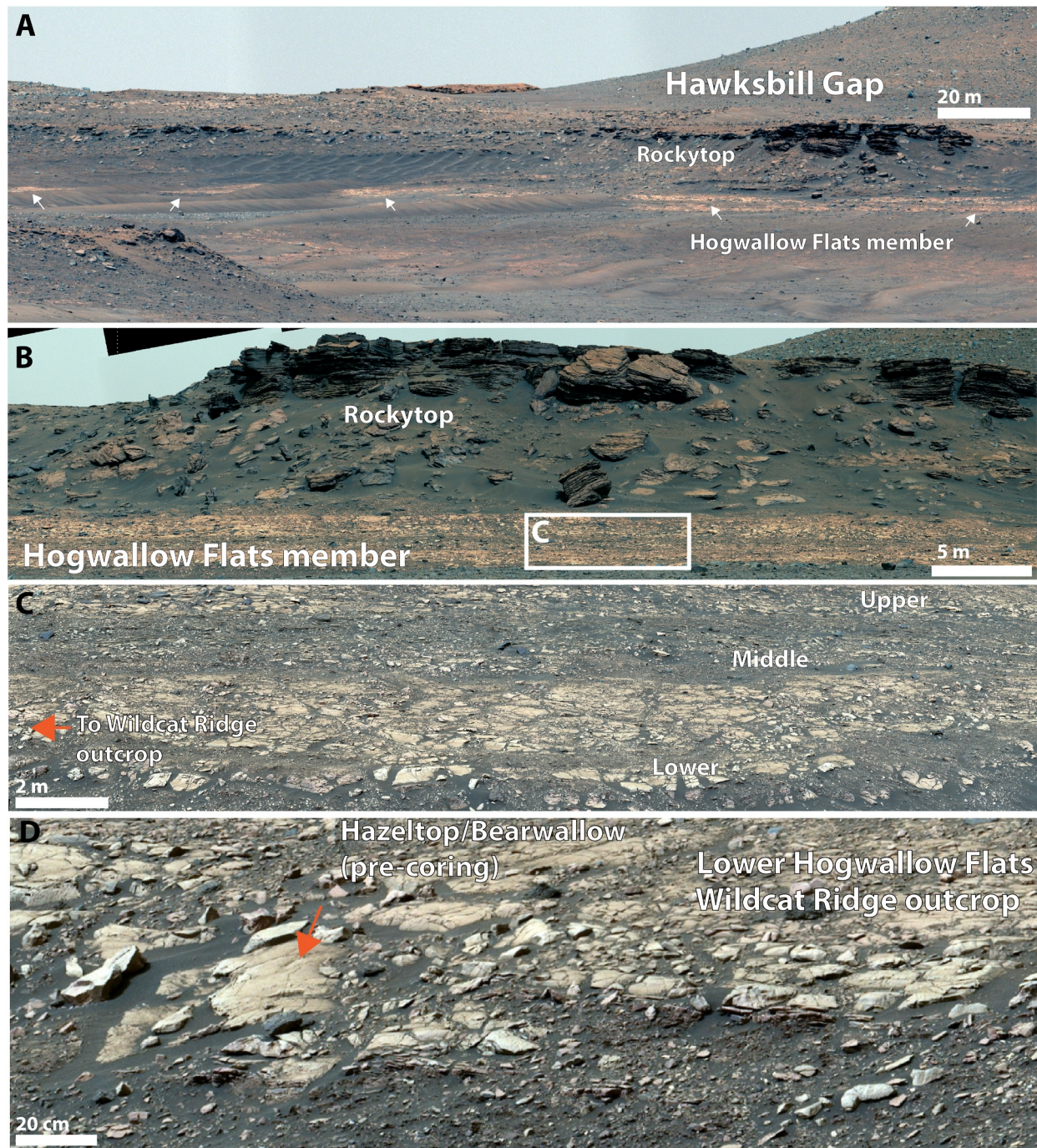


Figure 2. Mastcam-Z enhanced color landscape images of the Hogwallow Flats member of the Shenandoah formation. (a) Hawksbill Gap section of the Hogwallow Flats member indicated with white arrows (Sol 543, zcam08561); (b) Stratigraphic relationship between light-toned strata of the Hogwallow Flats Member and dark-toned rocks of the Rocky Top member at Hawksbill Gap (Sol 459, zcam08479); (c) Hogwallow Flats member showing alternating section of light-toned, platy strata overlying dark-toned, mottled and deformed strata (Sol 461, zcam08482); (d) Wildcat Ridge outcrop at lower Hogwallow Flats member showing pre-coring location for Hazeltop and Bearwallow sample cores (Sol 461, zcam08482).

Between Sols 505 and 628, *Perseverance* abraded three targets and collected three drilled sample cores from the Hogwallow Flats and Yori Pass members (Figure 4). The “*Uganik Island*” abrasion patch at Hidden Harbor revealed grain sizes at the boundary of mudstone/fine sandstone (Stack et al., 2024). *Uganik Island* at Hidden Harbor appeared to have a slightly coarser grain size than the Hogwallow Flats member abrasion patches at the Wildcat Ridge outcrop (“*Elkwallow Gap*” and “*Berry Hollow*”) (Benison et al., 2024).

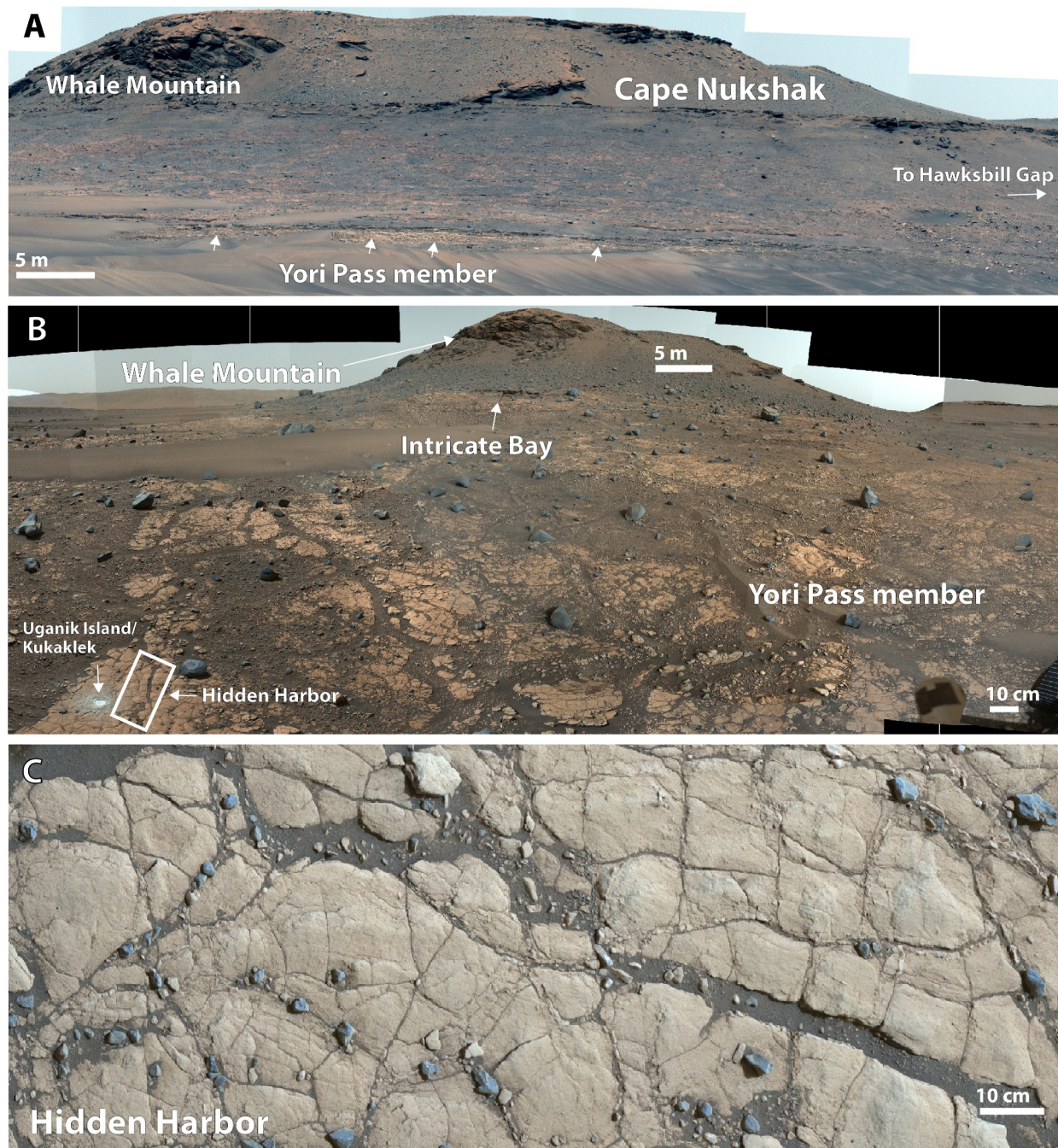


Figure 3. Yori Pass member at the Cape Nukshak section indicating light-toned strata (white arrows) (Sol 429, zcam08451); (a and b) Stratigraphic relationship between Yori Pass, Intricate Bay and Whale Mountain at the Cape Nukshak section (Sol 614, zcam08621); (c) Zoom of Hidden Harbor outcrop at the Yori Pass member showing fractured surface (Sol 610, zcam07101).

Hogwallow Flats drilled samples included a pair of samples at the Wildcat Ridge outcrop rock targets “*Hazeltop*” and “*Bearwallow*,” Figure 2d) and a single sample from the Yori Pass member (“*Kukaklek*”) (Bosak et al., 2024). These samples were collected because of the fine-grained texture, which could represent a depositional setting such as floodplain and/or pro-deltaic/lacustrine, and features indicating water-rock interaction and enhanced biosignature preservation potential (mottled colors, phyllosilicates, sulfates).

The depositional and diagenetic history of the rocks at Hogwallow Flats can provide insight into the habitability and biosignature preservation potential of this unit, which is critical for understanding the samples once they are

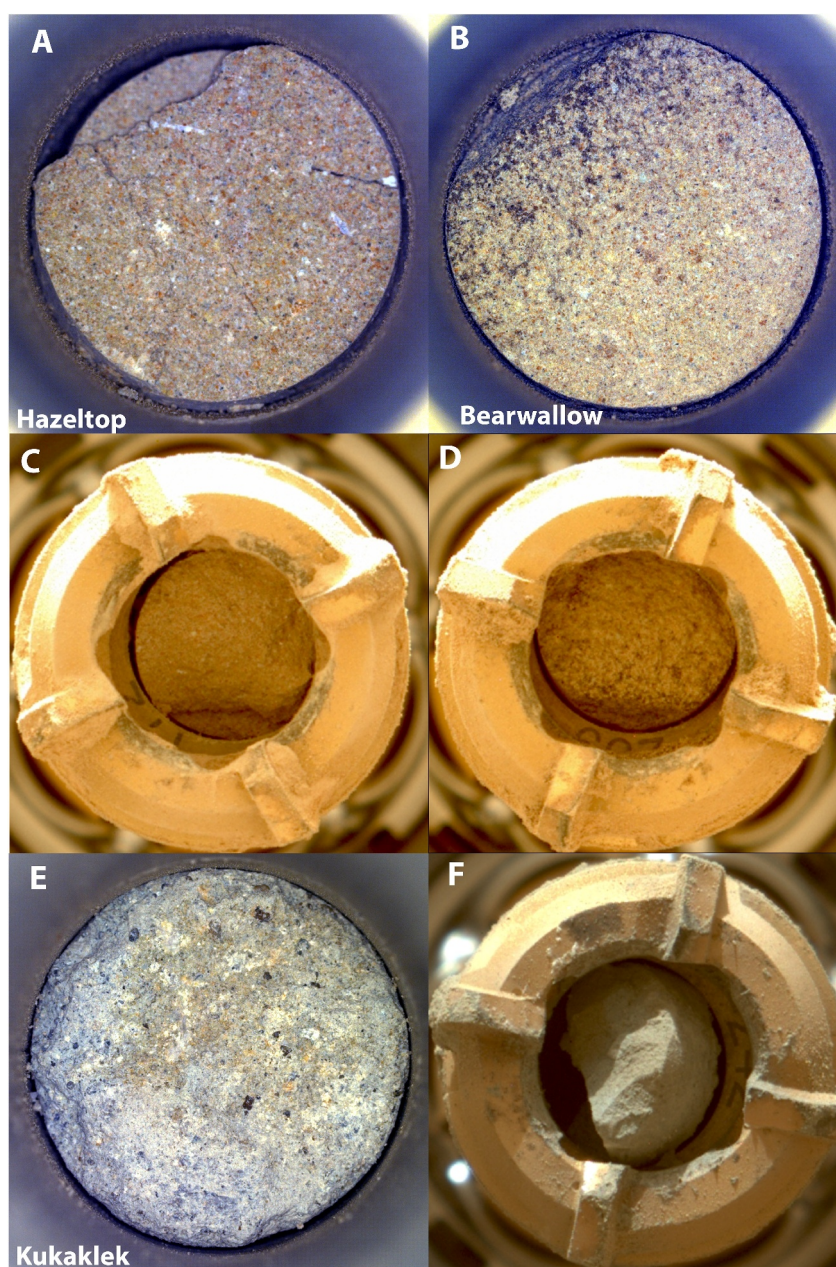


Figure 4. Rock cores collected by *Perseverance* rover from the Hogwallow Flats and Yori Pass members for Mars Sample Return. (a) Cachecam image (CCFC0509) (Maki et al., 2020) of Hazeltop core (Hogwallow Flats, Core #12); (b) Cachecam image (CCFC0516) of Bearwallow core (Hogwallow Flats, Core #13); (c) and (d), Mastcam-Z images of Hazeltop (Sol 509, zcam 05068) (c) and Bearwallow (Sol 509, zcam 05068) (d) cores in coring bit; (e) and (f) Cachecam image (CCF_0626) and Mastcam-Z image (Sol 626, zcam 05068) of Kukaklek core (Yori Pass, Core #14); The diameter of each rock core is 13 mm.

returned (Beatty et al., 2019; Meyer et al., 2022). Some forms of diagenesis are required for the preservation of organic carbon and other biosignatures (e.g., cementation, rapid mineralization, sulfurization of organic matter, polymerization). Others are associated with the destruction of biosignatures (e.g., late-stage groundwater flow, irradiation over geologic time scales, metasomatism). Thus, constraining the nature and timing of diagenesis is critical for interpreting the biosignature preservation potential of rock core samples. This work uses Mastcam-Z landscape and multispectral images as well as spectroscopic and geochemical data from the SuperCam instrument to interpret the sedimentary facies and diagenetic history of the Hogwallow Flats member. The objectives of this study were to: (a) constrain the diagenetic history of the Hogwallow Flats and Yori Pass members; (b) compare

diagenetic features in these rocks with past observations of similar features elsewhere on Mars; and (c) determine the implications of diagenesis for biosignature preservation in rock samples collected for MSR.

3. Data and Methods

3.1. Mastcam-Z: Landscape and Multispectral Images

Mastcam-Z (Mast camera - Zoom) is a pair of stereoscopic and multispectral cameras mounted on the mast of the *Perseverance* rover (Bell et al., 2021). The cameras have adjustable focal lengths and are equipped with CCD detectors with bonded Bayer filters at red-green-blue wavelengths (480/544/630 nm) (Bell et al., 2021). Additional narrowband filters in a filter wheel on each camera also allow for multispectral imaging in the visible/near infrared (442–1,022 nm) range at a total of 14 unique wavelengths. Calibration of Mastcam-Z images involves scaling to the radiance factor (I/F), where I is the unique scene radiance for a particular image, and F is the solar irradiance. Mastcam-Z acquires images of a rover-deck mounted calibration target and uses pre-flight calibration coefficients (Hayes et al., 2021) for ongoing calibration of multispectral images. Mastcam-Z spectra were converted to relative reflectance, R^* , by dividing I/F by the cosine of the solar incidence angle. Filters used in decorrelation stretches (DCS) of multispectral images presented here are from the left camera in visible wavelengths, L2 (754 nm) L5 (528 nm) and L6 (442 nm), and the right camera in near-infrared wavelengths R6 (1,022 nm), R3 (910 nm), and R1 (800 nm). Enhanced color images are Red: 630 nm, Green: 540 nm, Blue: 480 nm unless otherwise specified.

Mastcam-Z acquired 72 multispectral image sets and ~40 landscape mosaics during investigation of the Hogwallow Flats and Yori Pass members of the Shenandoah formation. These images were used to investigate the stratigraphic and diagenetic trends of Hogwallow Flats member. We used images from the well-exposed stratigraphy at Hawksbill Gap West to expand the detail of the Hogwallow Flats member at the Hawksbill Gap West stratigraphic column proposed by Stack et al. (2024). Spectral diversity of multispectral images was assessed with several techniques including enhanced-color combinations, decorrelation stretches in visible and near-infrared wavelengths, and spectral parameter maps (Bell et al., 2022; Horgan et al., 2023). Spectra from bedrock were extracted from regions of interest (ROIs) in multispectral images (Rice et al., 2022). Spectra from extracted ROIs were compared to laboratory mineral spectra convolved to Mastcam-Z filter bandpasses to aid in mineral identification (Figure S1 in Supporting Information S1). A list of Mastcam-Z images and sequence numbers are included in Table S1 in Supporting Information S1.

3.2. HiRISE Orbiter Images

The orbiter images used in this study (Figure 1) were from HiRISE (High-resolution Imaging System) (McEwen et al., 2007) at a 25 cm/pixel resolution. HiRISE color images were used in the construction of the Mars 2020 basemap (Ferguson et al., 2020; Stack et al., 2020) and images from this map were used to investigate outcrop morphology and lateral extent of the Hogwallow Flats and Yori Pass members.

3.3. SuperCam Spectroscopy

This study used the SuperCam instrument (Maurice et al., 2021; Wiens et al., 2021) and its range of remote sensing techniques, including visible/near-infrared (VISIR) spectroscopy (VIS: 0.40–0.85 μm , IR: 1.3–2.6 μm) (Fouchet et al., 2022) to assess mineralogy, time-resolved Raman spectroscopy (TRR) using a pulsed 532 nm laser also for assessing mineralogy, and laser-induced breakdown spectroscopy (LIBS) to measure major-element chemistry (Maurice et al., 2021).

SuperCam laser-induced breakdown spectroscopy (SuperCam LIBS) was used to measure the chemistry of bedrock (Table S2 in Supporting Information S1). The major element bulk chemistry measured by SuperCam LIBS was calculated after removing diagenetic features that do not represent bulk bedrock, such as veins or concretions (e.g., Dehouck et al., 2023). SuperCam LIBS collected data on these targets as well as a single dark-toned, mottled bedrock target on Sol 464 (Gimlet Ridge). No other observations were collected of the mottled bedrock due to engineering constraints (e.g., *Perseverance* could not perform proximity science or abrasion due to the small size of blocks (Figure 7a), so nearly all observations from the Hogwallow Flats were of the light-toned, tan-colored facies.

To further constrain the composition of the Hogwallow Flats and Yori Pass member bedrock, we used data from SuperCam's reflectance spectrometer to compare the relative shape and intensity of spectral features in the 1.3–2.6 μm region to laboratory spectra of Earth minerals using a linear spectral modeling approach, following the techniques used by Royer et al. (2023). This method estimates the possible mixture of mineral phases that best describes a given SuperCam IR spectrum using a weighted average of laboratory mineral spectra. Only the IR part of the spectra (1.3–2.6 μm) was modeled because nonlinear effects and scattering by atmospheric dust are more pronounced in the VIS wavelengths. Linear modeling of the data is based on a Bayesian method of parameter determination for the mixing model and was followed by statistical analysis using a Markov Chain Monte Carlo algorithm. This method draws upon the MELSUM (Multiple-Endmember Linear Spectral Unmixing Model, Combe et al., 2008) as well as the SMA (Spectral Mixing Analysis, Merényi et al., 1996) algorithms which fit a reflectance spectrum using a linear combination of reflectance spectra from laboratory derived reference libraries and/or from the data set itself. This method can determine the mineral phases that are most likely to describe the data and, therefore, likely to be present in the bulk mixture. However, the values of the mixing coefficients (i.e., their weighted average) are intended to describe only the similarity of a given spectrum to a combination of selected laboratory spectra (e.g., the endmembers) and are not related to the abundance of those minerals. As a result, quantitative mineral abundances are not determined using this method. The detailed methodology for the spectral modeling used here is included as Supporting Information S1.

3.4. SHERLOC and WATSON

We also used images from SHERLOC (*Scanning Habitable Environments with Raman and Luminescence for Organics and Chemicals*) and WATSON (Wide Angle Topographic Sensor for Operations and eNginEering). SHERLOC is a Deep UV (DUV, 248.6 nm *excitation laser*) fluorescence and resonance Raman spectrometer (Bhartia et al., 2021) and WATSON is a high-resolution imaging subsystem of SHERLOC. SHERLOC collects hyperspectral maps of natural and abraded surfaces to characterize the mineralogy of a target, using a laser scanner mirror to focus the 100 μm laser spot at each point within a map. Laser shot locations are registered to a monochromatic context image collected by the SHERLOC Autofocus and Context Imager (ACI). WATSON captures stand-alone observations of rock structures and textures from the outcrop to the grain scale (Minitti et al., 2019) and acquires color context imaging of SHERLOC and Planetary Instrument for X-Ray Lithochemistry (PIXL), a micro-X-ray fluorescence spectrometer onboard *Perseverance* (Allwood et al., 2020). It also captures high-resolution images to correlate the spatial distribution of organics and mineralogy detected by SHERLOC and the elemental maps generated by PIXL. For grain size approximations, we use previously published grain size measurements of Hogwallow Flats/Yori Pass bedrock derived from WATSON images of LIBS-cleared bedrock and abrasion patches (Stack et al., 2024).

4. Results

4.1. Sedimentology/Stratigraphy and Regional Context

At the Hawksbill Gap West traverse, three distinct facies were identified within Hogwallow Flats member (Figure 5), herein designated as Facies 1–3. Facies 1 is a dark-toned, purple/reddish mottled mudstone with deformed laminations. The grain size of this facies is inferred because it was never abraded or directly measured (see Stack et al., 2024). Facies 2 is a tan-colored, variably massive to laminated mudstone that forms a thin (~5–15 cm) cap over Facies 1. All of the abrasion patches and collection of drilled samples was performed in Facies 2. Facies 3 represents platy, low-angle cross-stratified fine sandstones, also with inferred grain size as grain size was not directly measured, but coarser grain size is suggested by the resistance to weathering compared to recessive layers of Facies 1.

There are three recognizable sub-members of the Hogwallow Flats member (Figure 6), herein designated the Lower, Middle and Upper Hogwallow Flats sub-members. The Lower Hogwallow Flats sub-member is composed of massive to laminated mottled mudstone of Facies 1 overlain by approximately 5–15 cm of Facies 2. The Middle Hogwallow Flats sub-member is typified by platy, low angle cross-stratified sandstones of Facies 3. Upper Hogwallow Flats is a combination of the massive to laminated mudstones of Facies 1 again overlain by approximately 5–15 cm of Facies 2.

At the Yori Pass member, Facies 1 and 2 were also observed at the Hidden Harbor outcrop. Here also the abrasion patch and core sampling activities were performed in Facies 2. Long-distance images of the Intricate Bay outcrop

Hawksbill Gap West

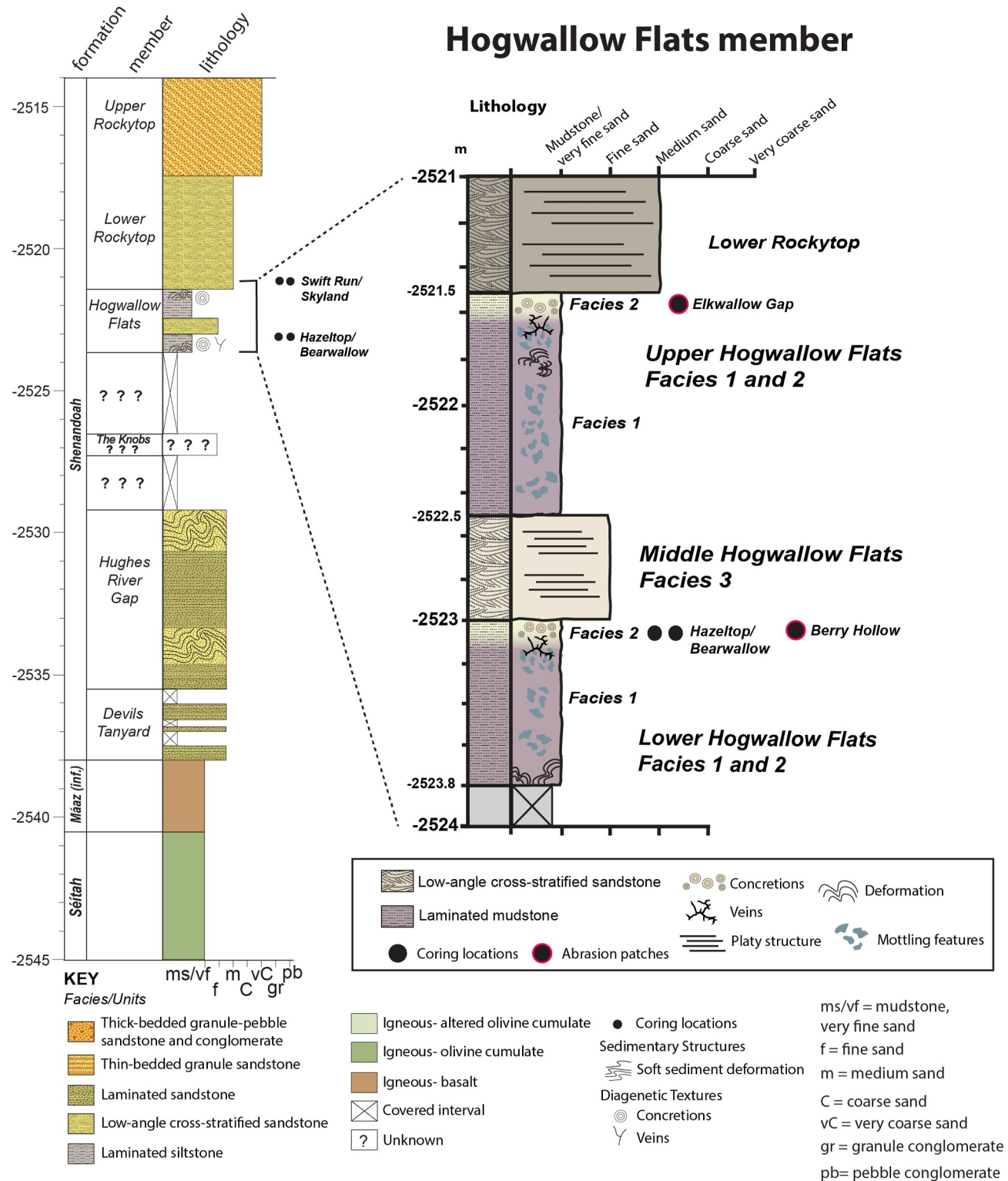


Figure 5. Stratigraphic column of the Hogwallow Flats member as seen from the Hawksbill Gap West traverse (Stack et al., 2024). Strata above and below the Hogwallow Flats member interval include the Rockytop, Hughes River Gap, and Devil's Tanyard members of the Shenandoah formation also described in Stack et al. (2024).

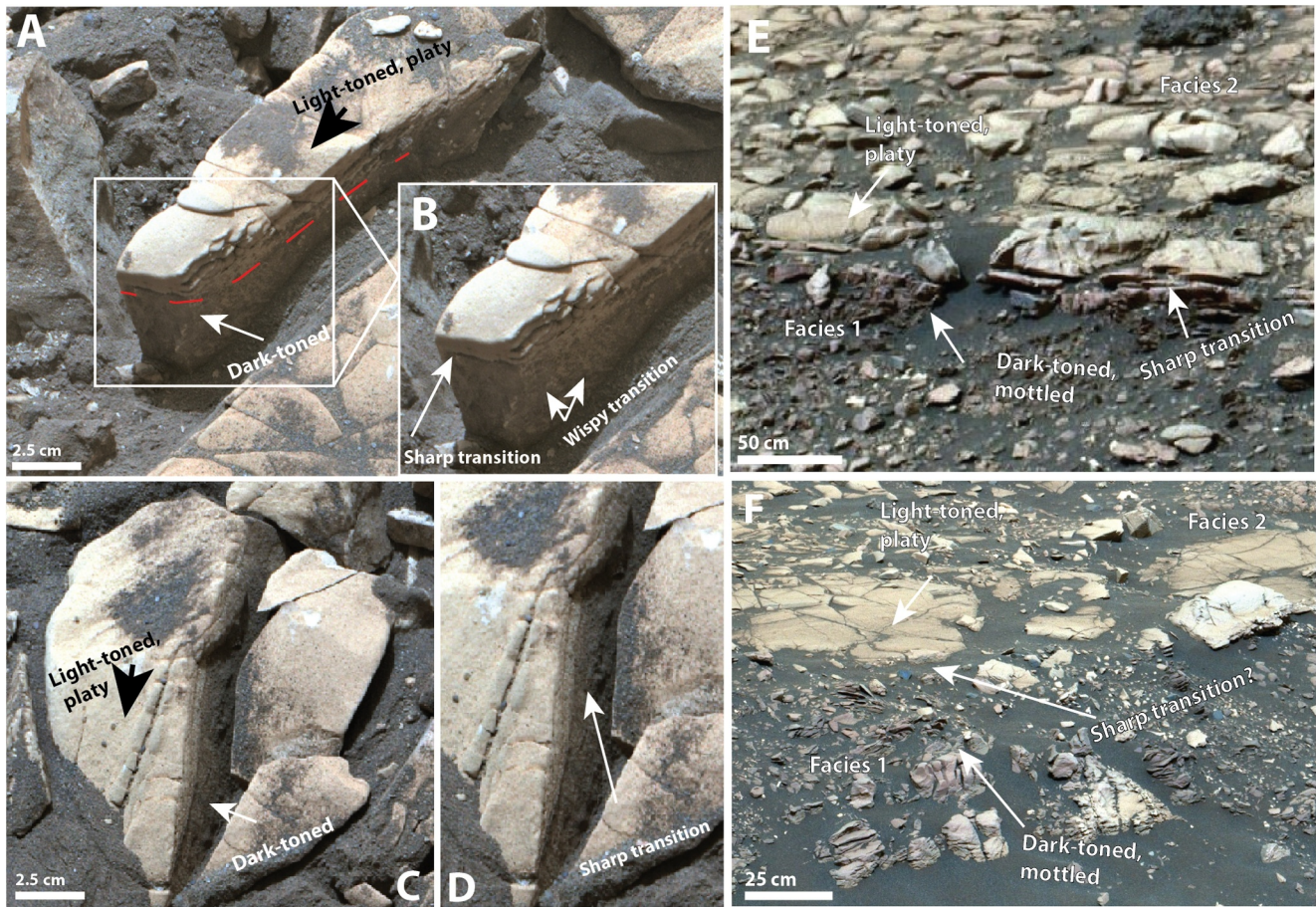


Figure 7. Transition between light-toned “cap” (Facies 2) and dark-toned, mottled and recessive outcrop (Facies 1) noted at the Yori Pass member in crushed bedrock from rover wheel track (a)–(d) and at outcrop scale (e)–(f) at the basal Hogwallow Flats member. (a) Rover-fractured bedrock at Moraine Creek outcrop (Yori Pass) showing transition (dashed red line) from light-toned, platy outcrop surfaces and dark-toned bedrock in subsurface of outcrops (imaged in shadow) (Sol 608, zcam 08617); (b) Zoom on transition showing both sharp and wispy, diffuse transitions between light and dark-toned bedrock; (c) and (d) Additional fractured bedrock at Moraine Creek, Yori Pass (Sol 608, zcam 08617) showing illuminated transition between light and dark-toned bedrock; (e) and (f) Outcrop-scale transition between light-toned, platy outcrop surface and dark-toned, mottled and recessive subsurface, a feature that was observed to be laterally continuous throughout the entire lower Hogwallow Flats outcrop (Sol 461, zcam08482). A 3D rendering of the Moraine Creek outcrop fractured bedrock (a)–(d) is available at <https://www.youtube.com/watch?v=7go9OewTSik>.

member 1 (Figures 7e and 7f), which is evidence for stratigraphic control on the changes in color (tan to red/gray mottled).

4.2. Long-Distance Spectral Properties

Mastcam-Z multispectral images demonstrate the spectral diversity of fan front strata and highlight the distinct spectral signature at Hogwallow Flats relative to other units at Hawksbill Gap (Figure 8). Decorrelation stretches (DCS) of visible wavelength images (442–754 nm) of the Hogwallow Flats member show a unique red/orange hue along strike that is distinct from strata above and below this interval, including the Rockytop, Hughes River Gap, and Devil’s Tanyard members of the Shenandoah formation (Figure 8). Red/orange colors in this decorrelation stretch are associated with Fe oxides and oxyhydroxides (Horgan et al., 2019) and here may include a complex mixture of ferrous/ferric sulfates (Hurowitz et al., 2023) and Fe oxides such as hematite (Mandon et al., 2024). Green and blue colors represent ferrous-iron-bearing minerals including olivine and/or pyroxene, which here dominate the regolith spectra (Vaughan et al., 2023). There are several regolith-covered intervals within the section, as well as dark-toned regolith and aeolian megaripples on the crater floor associated with Fe oxides (red colors) that stand in stark contrast to the magenta hues of bedrock exposed at Hughes River Gap and Devil’s Tanyard members, respectively.

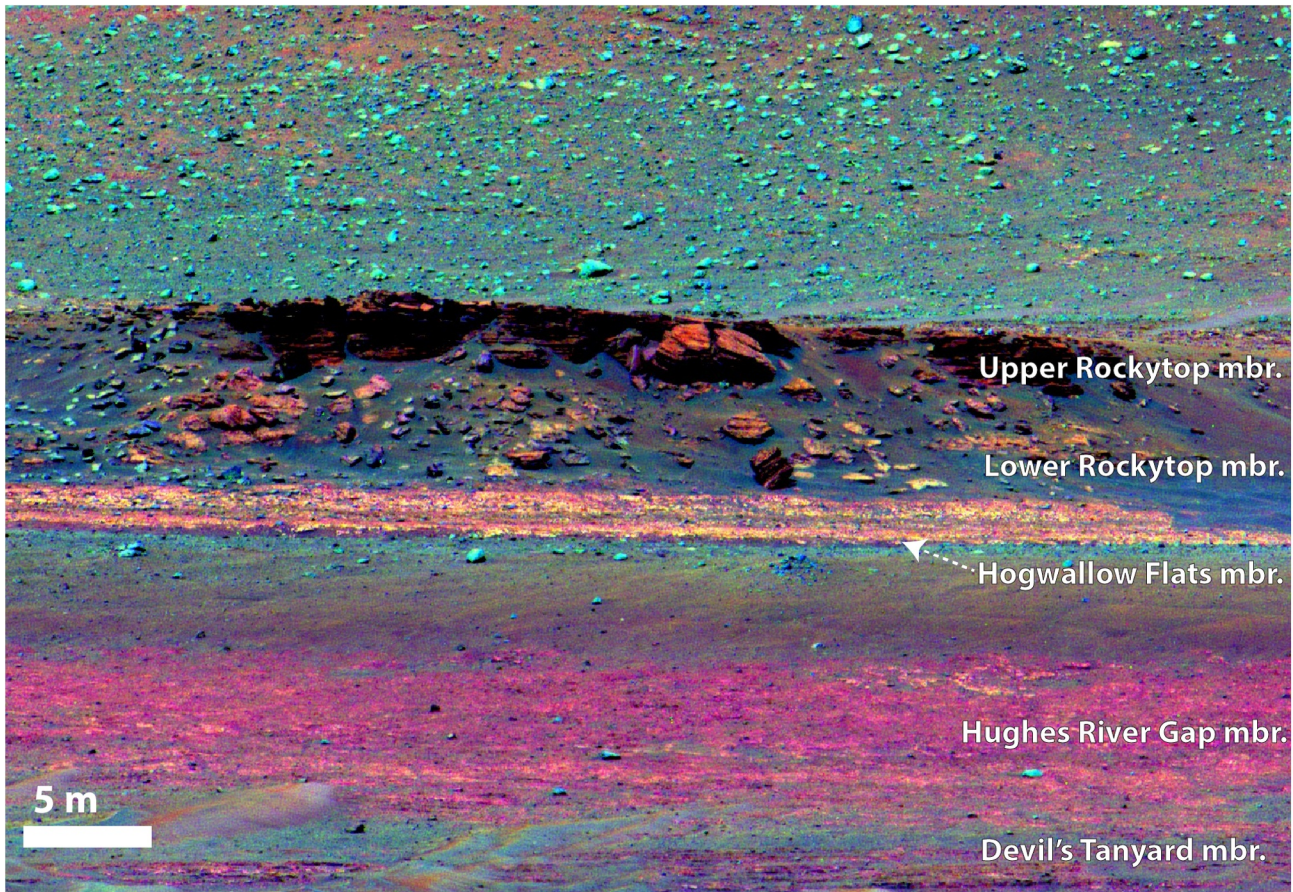


Figure 8. Visible wavelength decorrelation stretch (DCS) of Mastcam-Z image (Sol 676, zcam03518) demonstrating the spectral diversity of the Shenandoah formation near Hawksbill Gap showing stratigraphic members of the Shenandoah formation (from Stack et al. (2024)). Decorrelation stretch is L2 (754 nm) L5 (528 nm) and L6 (442 nm) where red, orange and magenta hues are associated with materials exhibiting variable states of oxidation and green to blue are ferrous minerals (e.g., olivine, pyroxene) combined with variable dust cover (Vaughan et al., 2023).

Mastcam-Z multispectral images of the Intricate Bay outcrop (Yori Pass member) revealed mottling features resembling the appearance of Facies 1 at Lower Hogwallow Flats (Figure 9). The visible wavelength DCS indicated major spectral differences between the overlying coarse sandstones, the tan outcrop surfaces (Facies 2), and the mottled, recessive facies (Facies 1). Tan outcrop surfaces appeared yellow to orange, similar to the long-distance observations of the Hogwallow Flats member. Mottling features appeared to show cm-scale variation in spectral properties, with colors ranging from purple to pink (ferric iron-bearing minerals) and areas of green (ferrous iron-bearing minerals) interspersed within several of the larger blocks in the lower portions of the stratigraphy.

4.3. Diagenetic Textures

4.3.1. Sulfate Cements and Millimeter-Scale Veins in Abrasion Patches From Facies 2

The matrix of the light-toned, laminated to massive mudstone of Facies 2 contains a mixture of Mg and Fe sulfate minerals with grains that are close to or below the limit of the resolution by WATSON (30 microns) (Figure 10a). Intergranular and pore-filling cements were observed in the abrasion patch at the Yori Pass outcrop (Uganik Island) (Figure S4 in Supporting Information S1) and to a lesser degree in the thin white venules at the Hogwallow Flats outcrop abrasion patches (Berry Hollow and Elkwallow Gap) (Benison et al., 2024). There appeared to be a greater proportion of sulfate cements in Facies 2 from Uganik Island compared to Facies 2 from Berry Hollow. There were also notable differences in the abundance and scale of small patches of light-toned veins identified as Ca sulfate (Benison et al., 2024). SuperCam Raman spectroscopy previously identified some of the Ca sulfates in the Uganik Island abrasion patch as anhydrite, based on comparisons with terrestrial anhydrite (Bosak et al., 2024;

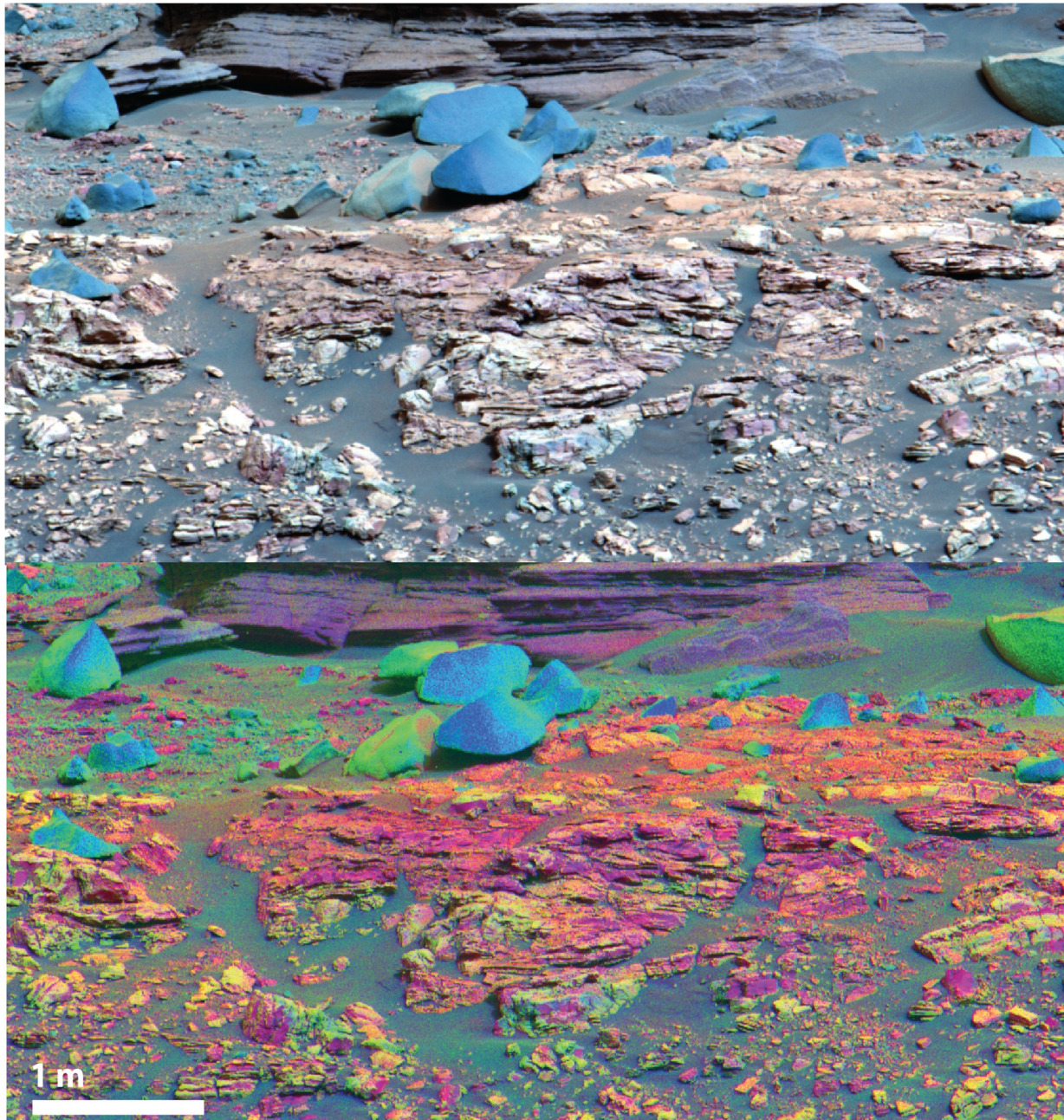


Figure 9. Mastcam-Z multispectral images of Intricate Bay, Yori Pass member (Sol 621, zcam 03488). Enhanced color (upper panel) is L2 (754 nm), L5 (528 nm), L6 (442 nm); Visible wavelength decorrelation stretch (bottom panel) is L2 (754 nm), L5 (528 nm), L6 (442 nm) where magenta hues are associated with materials exhibiting variable states of oxidation and green to blue are ferrous minerals (e.g., olivine, pyroxene) (Vaughan et al., 2023).

Lopez-Reyes et al., 2023). Uganik island has abundant light-toned, mm-scale filled veins and vugs whereas Berry Hollow lacks veins and vugs at the same scale and distribution. Differences in cements and grain sizes are likely related to the overall color of the abrasion patches. Colors were distinct between the abrasion patches, but Berry Hollow had a mottled pink and tan appearance in both natural and enhanced color images, whereas Uganik Island also appeared mottled but was overall darker in tone, contained larger light-toned veins and vugs, and had larger, coarser grains rimmed by dark-toned cements.

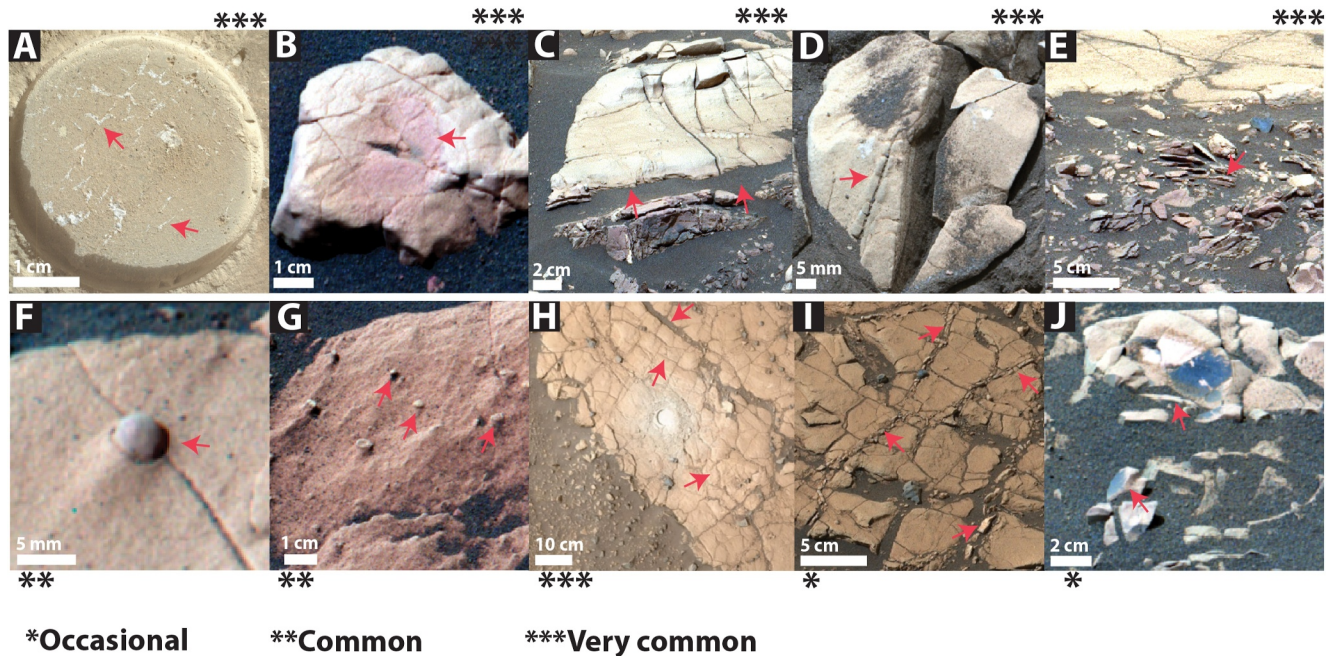


Figure 10. Diagenetic textures observed at the Hogwallow Flats and Yori Pass members as seen by Mastcam-Z (enhanced color). (a) Light-toned sulfate cements in Uganik Island abrasion patch at the Hidden Harbor outcrop, Yori Pass (Sol 607, zcam 03487) showing small-scale fractures filled with light-toned material; (b) “Peters Point” float block at the lower Hogwallow Flats submember (Sol 503, zcam 03404) showing red toned bedrock of Facies 2; (c) Transition between light-toned (Facies 2) and dark-toned bedrock (Facies 1) at the lower Hogwallow Flats sub-member (Sol 461, zcam 08482); (d) Centimeter-scale light-toned “cap” (Facies 2) over dark-toned matrix (Facies 1) in fresh face of Yori Pass member bedrock fractured by rover wheel at Moraine Creek (Sol 608, zcam08617); (e) Deformed, recessive bedrock observed in Facies 1 at the lower Hogwallow Flats member (Sol 461, zcam 08482); (f) Hematite-bearing concretion at Pignut Mountain outcrop (Kalucha et al., 2024), lower Hogwallow Flats submember (Sol 464, zcam 03378); (g), Wind-abraded concretions at Peters Point, upper Hogwallow Flats sub-member (Sol 503, zcam 03404); (h) 3D model of Hidden Harbor outcrop (Yori Pass) generated from Mastcam-Z stereo images (Tate et al., 2023) showing Uganik Island abrasion patch and extensive fracturing; (i) Calcium sulfate-filled polygonal fractures at Hidden Harbor, Yori Pass (Sol 614, zcam08622); (j) Dark-toned rock coating (Lanza et al., 2023) at Hogback Mountain outcrop, Hogwallow Flats member (Sol 523, zcam 03417). Asterisks indicate relative frequency of occurrences observed in Mastcam-Z landscape images and mosaics.

4.3.2. Centimeter-Scale Calcium Sulfate Veins in Facies 2

Some of the cm-scale fractures of Facies 2 are filled with a light-toned mineral phase identified as Ca sulfate, likely anhydrite (Bosak et al., 2024; Lopez-Reyes et al., 2023; Nachon et al., 2023; Phua et al., 2024) (Figure 10). Ca sulfate veins follow polygonal fracture networks at the outcrop scale and occasionally cut through networks of unfilled, cm-scale fractures. Vein widths vary from millimeters to several centimeters (Nachon et al., 2023). Several veins with diameters of up to 10 cm were noted at the Hogwallow Flats member. Not all fractures are filled with Ca sulfate veins, as the majority of the polygonal fractures were unfilled and represent present void space. This was the case for both Hogwallow Flats and Yori Pass members. There did appear to be a larger proportion of sulfate-filled fractures at the Yori Pass member (Hidden Harbor outcrop) (Figure 10i) compared to the Hogwallow Flats member (Wildcat Ridge outcrop).

4.3.3. Dark-Toned Coatings on Facies 1 and 2

Dark-toned rock coatings were identified at the Hogwallow Flats and Yori Pass members (Figure 10j). Prominent examples include the Hogback Mountain target at Hogwallow Flats (Figure S5 in Supporting Information S1) and the Hidden Harbor outcrop at Yori Pass. Dark-toned coatings were observed on both light-toned bedrock (Facies 2) and red-purple-gray mottled bedrock (Facies 1). In some cases, the dark-toned coatings were associated with the mottling features, suggesting that these coatings may contribute to the mottled appearance of bedrock. There were no coatings noted in Facies 3 (middle Hogwallow Flats sub-member). These surfaces are enriched in Mn and have been interpreted in Facies 2 as a desert varnish-like rock coating (Lanza et al., 2023).

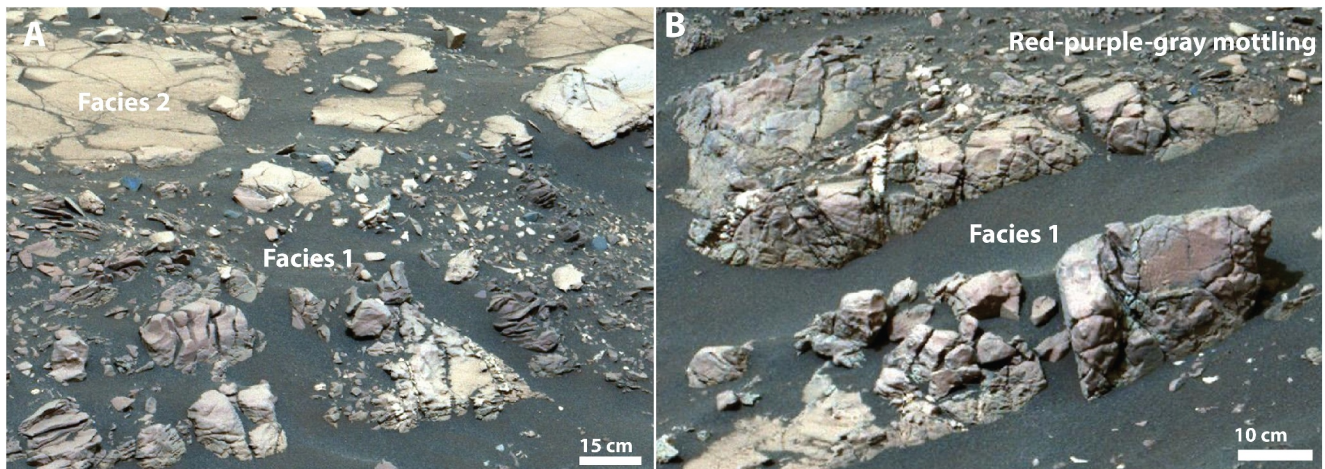


Figure 11. Red-purple-gray mottling features observed at the lower Hogwallow Flats sub-member (a–b) (Sol 461, zcam 08482) showing the transition from light-toned bedrock (Facies 2) to red-purple-gray mottled bedrock (Facies 1).

4.3.4. Concretions in Facies 2

Concretions were observed throughout Hogwallow Flats and Yori Pass (Figures 10f and 10g). Notably, these features were restricted to light-toned mudstones of Facies 2 and were not observed in the dark-toned, mottled Facies 1. A variety of rounded, discoidal to spheroidal concretions were observed in Mastcam-Z images from upper Hogwallow Flats. In several cases, fractures cross-cut concretions, implying that fracturing occurred after the concretions formed (Figure S5 in Supporting Information S1). Some of the concretions were attached to the host bedrock by a thin erosional remnant. A small concretion at Pignut Mountain (lower Hogwallow Flats member) observed by Mastcam-Z appeared to have a Fe oxide signature similar to the host bedrock of Facies 2 (Figure S6 in Supporting Information S1). Facies 2 at the Upper Hogwallow Flats sub-member appeared to have a greater density of concretions relative to the lower Hogwallow Flats sub-member and Yori Pass (Kalucha et al., 2024).

4.3.5. Potential Soft Sediment Deformation Features in Facies 1

Within Facies 1, thin laminations appear to be disaggregating into small (~10 cm wide) chips of varying orientation (Figure 10e). Some of these features have a curvilinear orientation and resemble soft sediment deformation features (Lesh et al., 2023). These features were most apparent in the lower Hogwallow Flats sub-member and appeared minimal at upper Hogwallow Flats. However, such features were absent in light-toned outcrop (Facies 2) that contained concretions. These features were also identified from long-distance images of the Intricate Bay outcrop at the Yori Pass member (Figure 9) where they appeared similar to those observed at the Hogwallow Flats member.

4.4. Mottling Features

A distinct interval of dark-toned, mottled and recessive outcrop (Facies 1) was observed at the Hogwallow Flats and Yori Pass members that underlies the tan, light-toned, laminated to massive mudstones of Facies 2 (Figure 11). At the lower Hogwallow Flats sub-member, the mottling in Facies 1 was most prominently demonstrated on apparently massive blocks of bedrock with no laminations.

Visible and near-infrared decorrelation stretches of Mastcam-Z images enhance the color differences between Facies 1 and 2 at Hogwallow Flats (Figures S7 and S8 in Supporting Information S1) and Yori Pass (Figure S9 in Supporting Information S1). There is a distinct transition observed in nearly all images between the light-toned, fine sandstones of Facies 2 and the darker-toned, red-purple-gray mottled Facies 1 stratigraphically below. This transition in spectral properties was observed both at the outcrop-scale (Figures S7–S9 in Supporting Information S1) and at the cm-scale during collection of drilled rock core samples.

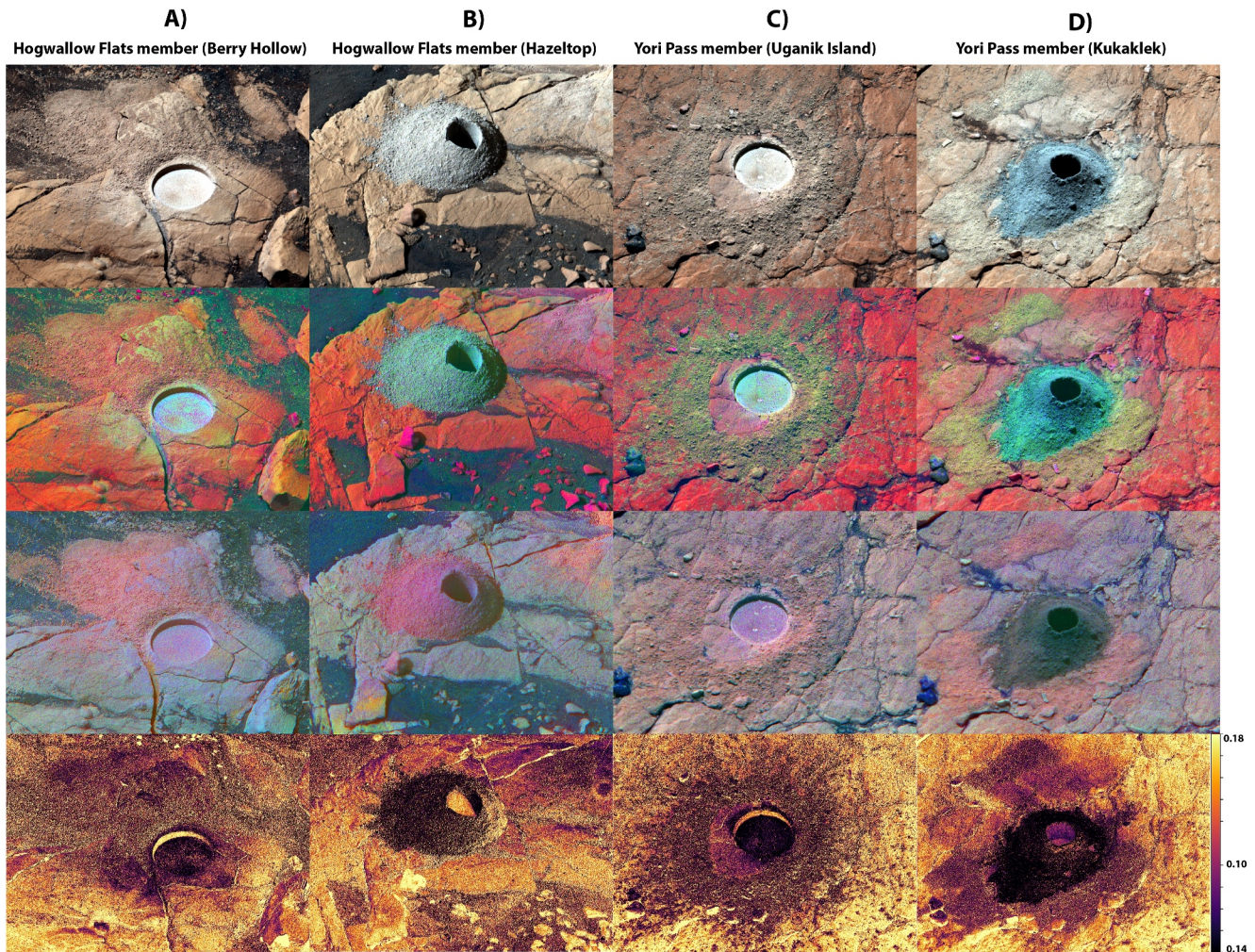


Figure 12. Multispectral observations of abrasion patches and drill core tailings from the Hogwallow Flats and Yori Pass members. (a) Berry Hollow abrasion patch (Hogwallow Flats member) (Sol 505, zcam 03405; B) Hazeltop drill core tailings (Hogwallow Flats member) (Sol 512, zcam 03408); (c) Uganik Island abrasion patch (Yori Pass member) (Sol 619, zcam 03487; D) Kukaklek drill core tailings (Yori Pass member) (Sol 628, zcam 03406). Enhanced Color is L0R (630 nm), L0G (544 nm), L0B (480 nm); Decorrelation stretch (visible) is L2 (754 nm), L5 (528 nm), L6 (442 nm) where red, orange and magenta colors are indicative of Fe oxides and blues, greens and purples indicate pyroxene/olivine; Decorrelation stretch (near-infrared) is R6 (1,022 nm), R3 (910 nm), R1 (800 nm) where pink, beige and purple are indicative of Fe oxides and blue/purple of pyroxene and/or olivine; Band depth parameter map is 528 nm band depth and shoulders (442 nm, 605 nm), with lighter-toned colors indicating more ferric material and darker-toned colors indicating less ferric material (e.g., oxidation state map); 528 nm band depth values range from 0.04 (dark tones) to 0.21 (light tones). All images were acquired within 2 hr of local solar noon to minimize concerns regarding photometric variations among the scenes.

4.5. Spectral Properties of Abrasion Patches and Collection of Drilled Samples

Enhanced color images, decorrelation stretches, and band parameter maps show distinct differences between natural surfaces, abraded surfaces, and drill core tailings. Mastcam-Z multispectral image products of abrasion targets and drill core tailings are shown in Figure 12. These differences are indicative of differences in mineralogy, composition, and redox state. One key difference between the samples was that the abrasions and tailings of the Yori Pass member show a much less red hue compared to the natural surface and are distinctly darker in color compared to the Hogwallow Flats member abrasions/tailings, as quantified in Figure 13.

The 528 nm band depth parameter maps indicated differences in redox state between natural surfaces, abraded surfaces, and drill core tailings, with notable differences between drill tailings at the Hogwallow Flats and Yori Pass members (Figure 12). These maps have been interpreted as a proxy for bulk redox state, with larger 528 nm band depth values representing stronger signatures of Fe^{3+} - or Mn^{2+} - bearing phases and thus more oxidized material (Rice et al., 2022). All abraded surfaces and drill tailings had lower 528 nm band depth values and were less ferric (darker colors) relative to surface materials (lighter colors). Most notable are the depleted 528 nm band

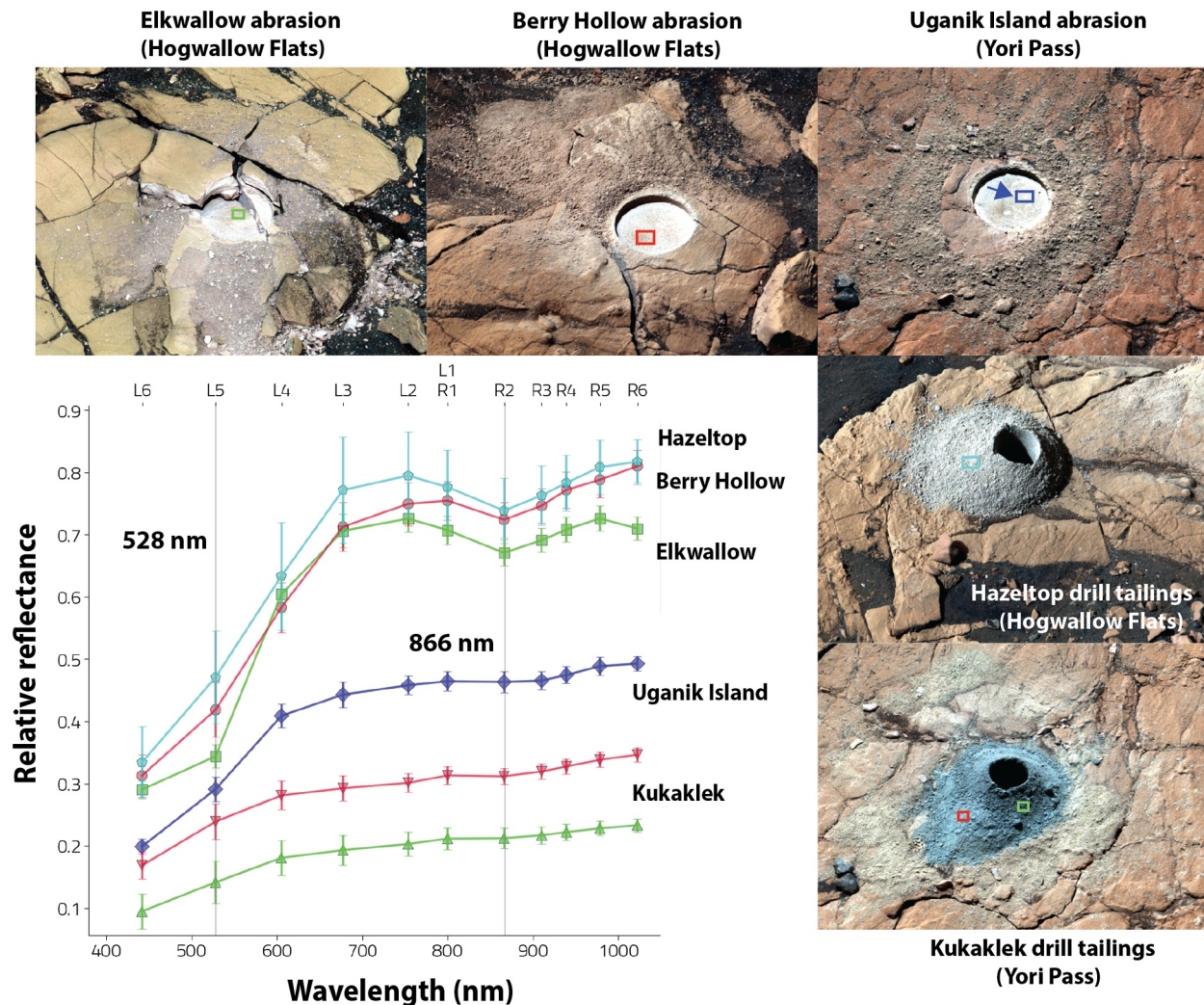


Figure 13. Multispectral observations of abrasion patches and drill core tailings at the Hogwallow Flats and Yori Pass members showing potential differences in redox state (528 and 866 nm bands indicating oxidation). From upper left to lower right (Enhanced color images): Elkwallow Gap abrasion, Hogwallow Flats (Sol 472, zcam03384); Berry Hollow abrasion, Hogwallow Flats (Sol 505, zcam 03405); Uganik Island abrasion, Yori Pass (Sol 619, zcam03487); Hazeltop borehole and tailings (Sol 512, zcam 03408); Kukaklek borehole and tailings (Sol 628, zcam 03492). Reflectance spectra are offset by 0.01 per spectrum. Abrasion patches and boreholes are approximately 5 and 1.3 cm in diameter, respectively.

depth values and subsequent dark black colors (Figure 12) in the Kukaklek core tailings compared to those of the Hazeltop tailings, which further suggests differences in color of the tailings are not due to photometric effects but instead differences in composition and/or oxidation state.

Red to orange colors in the visible-wavelength decorrelation stretch (Figure 12, second row) are associated with Fe oxides and oxyhydroxides (Horgan et al., 2019; Rice et al., 2023). In these image products, dusty surfaces appear as orange to red, whereas more strongly oxidized surfaces appear pink (Mandon et al., 2024). Green and blue colors represent ferrous-iron-bearing minerals including olivine and/or pyroxene (Vaughan et al., 2023). In the near-infrared decorrelation stretch (Figure 12, third row) pink, beige and purple are indicative of Fe oxides and blue/purple of pyroxene and/or olivine.

Variations in Fe content, mineralogy and/or redox state between the two sample sites indicated significant differences in spectra from both the abrasion patches and borehole tailings (Figure 13). Abrasion patches and tailings from the Hogwallow Flats member show co-occurring strong 528 and 866 nm bands, suggesting finely crystalline hematite (Figure 13) (Burns, 1993; Haber et al., 2022; Morris et al., 2006; Rudolph et al., 2022). In particular, the

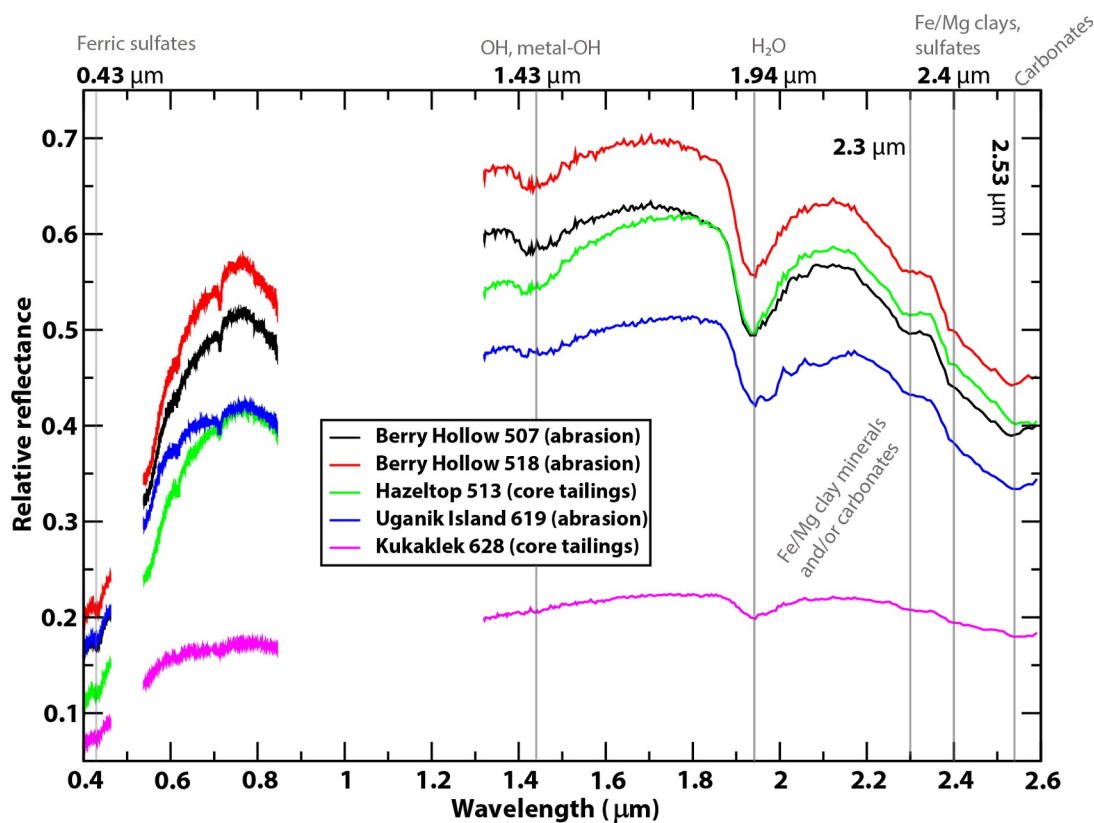


Figure 14. Average SuperCam visible and infrared (VISIR) spectra from abraded patches and core tailings at Hogwallow Flats (Berry Hollow, Hazeltop) and Yori Pass (Uganik Island, Kukaklek). Gray vertical lines indicate positions of important absorption bands at 0.43 μm (ferric sulfates), 1.43 μm (OH, metal-OH), 1.94 μm (water), 2.30 μm (Fe/Mg phyllosilicates and/or carbonates), 2.40 μm (sulfates/phyllosilicates), and 2.53 μm (carbonates).

abrasion patch at Elkwallow Gap has deep 528 and 866 nm bands (Figure 13) that closely resemble laboratory spectra of nanophase ($>10 \mu\text{m}$) red hematite (Figure S1 in Supporting Information S1). The Elkwallow Gap abrasion also shows a unique downturn (negative slope) between 978 and 1,022 nm. Overall, Elkwallow Gap with its sharp 528 and 866 nm bands appears to be the sample with the strongest Fe^{3+} signature. By contrast, the 528 and 866 nm bands were comparatively minor at the Yori Pass abrasion (Uganik Island) and altogether absent in Kukaklek tailings.

SuperCam visible/infrared (VISIR) spectra from Hogwallow Flats and Yori Pass (Figure 14) exhibit signatures of Fe/Mg phyllosilicate clay minerals and Fe/Mg sulfates, along with Ca sulfates in veins and voids (Bosak et al., 2024; Dehouck et al., 2023; Nachon et al., 2023). The 0.43 μm feature indicates the presence of ferric sulfates (Johnson, Wiens, et al., 2023) and hydration features at 1.9 and 2.3 μm indicate the presence of Fe/Mg-phyllosilicates and other hydrated minerals (Dehouck et al., 2023). Mineral phases detected with additional instruments and techniques (SuperCam Raman, SHERLOC Raman, PIXL XRF) include hydrated and anhydrous sulfate minerals, phyllosilicates such as nontronite or saponite, ferric sulfates, Ti/Cr oxides, and grains of kaolinite/montmorillonite (Bosak et al., 2024; Phua et al., 2024).

Modeling of the infrared region of the IR spectra identified candidate minerals that are likely to be present in abrasion patches and drill core tailings at the Hogwallow Flats and Yori Pass members (Figure 15). A comparison with natural surfaces (Moraine Creek, Intricate Bay, Lefthand Hollow, and Gimlet Ridge) is also presented. Potential mineral phases across all observations include Fe sulfates, anhydrite, Fe/Mg phyllosilicates, carbonates, Fe hydroxides, as well as olivine and pyroxene (Figure 15). Interestingly, Gimlet Ridge is the only target on the dark-toned, mottled bedrock, and this target shows more limited spectral contributions from Fe-sulfates and Fe-hydroxides.

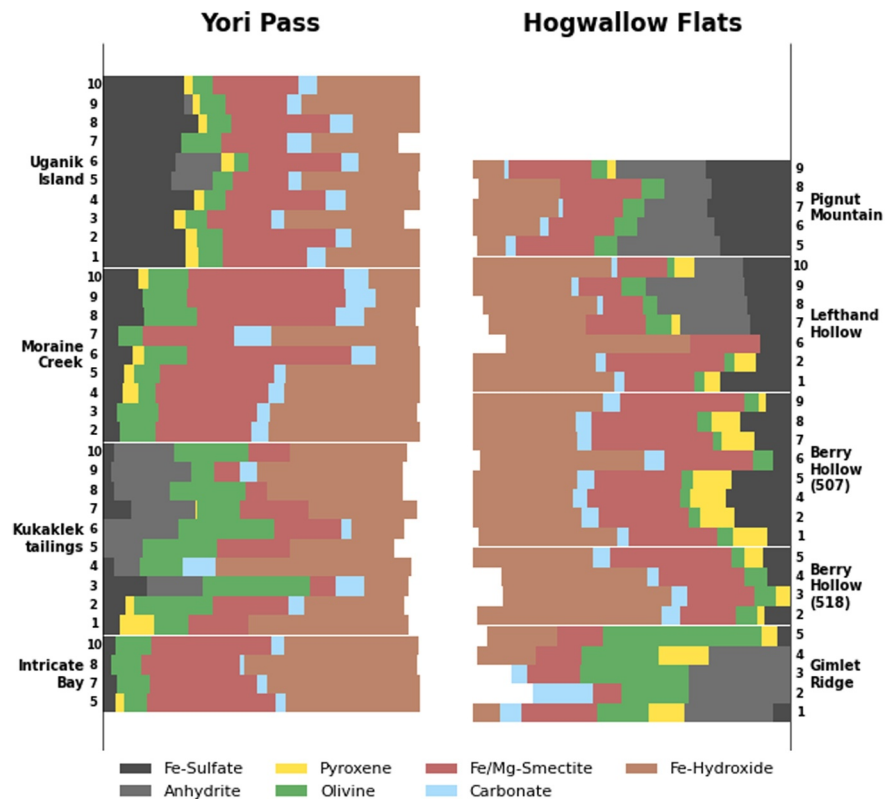


Figure 15. Possible mineral mixtures present in Hogwallow Flats and Yori Pass member targets inferred from modeling of SuperCam infrared (IR) spectra. Relative mineral mixing coefficients (unrelated to mineral abundance) derived by near-IR spectral modeling of SuperCam spectra from Hogwallow Flats and Yori Pass members. Each color corresponds to a mineral family and the length of the bar represents the value of each mixing coefficient whose sum is normalized to 1. Blanks are coefficients whose likelihood is lower than 1 and thus, considered as not present (see Supporting Information S1). Numbers on each side are the SuperCam IR raster positions for each target. Points in regolith, thick dust, or shadows were not included.

5. Discussion

5.1. Evidence for Diagenesis in the Hogwallow Flats and Yori Pass Members

Diagenetic features and textures observed within the Hogwallow Flats and Yori Pass members include fine-grained crystalline red hematite, red-purple-gray mottling, concretions, Fe and Mg sulfate-cemented bedrock, occasional Ca sulfate veins, soft-sediment deformation, and dark-toned rock coatings. While some of these features, such as the concretions, could have formed at any time (either early or late; e.g., Sun et al., 2019; Stack et al., 2014), we are able to better constrain the relative time of formation of other features, such as the distinct color changes. However, assumptions about diagenesis require first ruling out that color changes could have been a result of depositional processes.

5.1.1. Variations in Color: Depositional or Diagenetic?

The color changes between Facies 1 and 2 observed both at the sub-meter scale and laterally along tens of meters of outcrop (Figures 9–11) could have resulted from depositional processes. In this way, the distinct color changes between the light-toned, platy rocks at outcrop surfaces (Facies 2) and the dark-toned recessive bedrock below (Facies 1) may represent an unconformity, a change in grain size, or a change in composition of sand and/or cement. If not a result of deposition, this color change between Facies 1 and 2 could be due to diagenesis. Distinguishing between these hypotheses is challenging because nearly all of the contacts between Facies 1 and 2 were obscured by regolith and dark-toned sand.

Focusing on color variations within Facies 1, the cm-scale color transitions from red to purple to gray that represent mottling features are clearer in many cases (Figure 11), so we are better able to constrain the origin of

these features. Detailed observations of Facies 1 strata with patchy red-purple-gray areas support the hypotheses that these color changes are a result of diagenesis rather than depositional processes. For example, sedimentary structures and textures do not change within Facies 1. Further, Mastcam-Z multispectral images reveal color variations that cross cut the laminations of Facies 1 and diffusely rather than sharply transition in color. Other smaller areas with sharper transitions to a gray color are more consistent with rock coatings rather than inherent colors of the matrix. Zooming out to the outcrop-scale color transition between Facies 1 and 2 (Figures 6 and 7), the distinct color transition laterally across tens of meters of outcrop suggest that this color transition may be stratigraphically controlled rather than a surficial feature such as a rock coating. Thus, we favor the hypothesis that color variations within Facies 1 were a result of diagenesis.

5.1.2. Comparisons With Earth Analogs: Early or Late Diagenesis?

Comparisons with Earth analogs can be useful for constraining the origin of mottling observed within both the Hogwallow Flats and Yori Pass members. One of the most common formation mechanisms of terrestrial mottled mudstones is from syndepositional/early diagenetic alteration due to water table fluctuations. This tends to occur during or shortly after deposition and before lithification in near-surface environments from the oxidation and reduction of Fe-bearing phases (Kraus & Aslan, 1993; PiPujol & Buurman, 1994; Song et al., 2018). Mottling is common in clay-rich, periodically waterlogged sediments subject to a strongly fluctuating water table, leading to iron mobilization and reprecipitation as the source of the reddish purple-gray colors (Driese et al., 1995, 2018; Kraus & Aslan, 1993). Such poorly compacted, clay mineral-rich sediment allows for the formation of extensive redoximorphic features that can lead to a mottled appearance. When buried, these distinct features can be preserved over geological time scales. Early diagenetic mottling is well preserved in terrestrial ~1.8 Ga alluvial and lacustrine paleosols (Driese et al., 1995). Because lithification greatly attenuates or terminates hydraulic conductivity in terrestrial mudstones (Driese et al., 1995; Gerhard, 2000), susceptibility to late-stage fluid flow can be minimal, meaning the mottled matrix of terrestrial mudstones can be preserved intact over geological time scales (see Supplementary Discussion).

If the red-purple-gray mottling of Facies 1 is a result of aqueous alteration from a fluctuating water table, then, based on terrestrial analogs, then we could expect a disruption of sedimentary features (Potter-McIntyre et al., 2014), variable redox state and Fe crystallinity at the centimeter to meter scale (Metcalfe et al., 1994), authigenic finely crystalline Fe oxides and clay minerals (Lepre & Olsen, 2021), a stratigraphic control on the location of mottling features (e.g., a horizon), and an absence of alteration features following late-stage fractures or faults, such as Liesegang banding or alteration haloes (Eichhubl et al., 2004). All of these features, minus banding or alteration haloes, were observed in Facies 1.

If the mottling features are instead due to late diagenetic fluid flow, then we could expect associated features such as a coarsening of hematite (Chan & Parry, 2000; Cornell & Schwertmann, 2003), the presence of a bleached zone or weathering front (Eichhubl et al., 2004), and extensive cross-cutting networks of filled fractures (Kronyak et al., 2019). In the case of a later alteration by Mg sulfate-rich brines, the destruction of authigenic clay minerals (Bristow et al., 2021) could also be expected. In this scenario, a later fluid flow event through more permeable conduit such as the coarse-grained sandstones stratigraphically above the Hogwallow Flats member could have enabled alteration by a late diagenetic weathering front. Characteristic bleaching can occur from repeated Fe dissolution-precipitation reactions under acidic conditions, as inferred from terrestrial settings (Parry et al., 2004). However, this would have resulted in the recrystallization of hematite to coarser grain size (Horgan et al., 2019), and presumably would have removed Fe/Mg bedrock sulfates detected by PIXL (Hurowitz et al., 2023), both of which were not observed. Additionally, strong spectral signatures of Fe/Mg phyllosilicate clay minerals in bedrock targets from Hogwallow Flats/Yori pass (Dehouck et al., 2023), also noted on concretions (Kalucha et al., 2024) are indicative of limited late diagenetic fluid flow (Rudolph et al., 2022), as these phases are also susceptible to destruction by later fluid flow in the case of Mg-sulfate rich brines (Bristow et al., 2021). While we cannot rule out the influence of late diagenesis altogether, the properties of this interval of the Shenandoah formation are more consistent with early diagenetic processes.

5.1.3. Red Color From Late Diagenesis?

Red colors in terrestrial mudstones/claystones can also result from late diagenetic “burial reddening” due to the dehydration of goethite and/or ferrihydrite to hematite, which can be a result of heating during burial

(Retallack, 1991; Spinola et al., 2018). This process reddens an originally brown or gray-colored mudstone toward a brick-red color (Blodgett et al., 1993). Burial reddening is therefore one explanation for the mottling, but it is unlikely that the Hogwallow Flats or Yori Pass members were buried by significant amounts of overburden that would generate the heat envisaged to drive burial reddening of goethite to hematite ($\sim 100\text{--}150^\circ\text{C}$) (Spinola et al., 2018). On the other hand, ferrihydrite can dehydrate to finely crystalline hematite at much shallower (<100 m) burial depths and ambient temperatures (Spinola et al., 2018), which may have contributed to the overall reddening of Facies 1.

5.1.4. Constraining the Depth of Burial

Compared to the 4–5 km depth of Gale crater, at approximately 1,600 m deep Jezero crater is comparably shallower, potentially leading to major differences in the total amount of overburden that may have once buried the strata of the Jezero fan sediments. If these rocks were deeply buried by multiple kilometers of overburden, then evidence of deep burial could include tectonic deformation, extensive networks of filled fractures that cross cuts stratigraphy, zeolitization of poorly crystalline phases, and/or illitization of smectite (Novoselov et al., 2015). Tectonic deformation, extensive filled fractures that cross-cut stratigraphy, and the presence of illite are recognizable with *Perseverance's* instrument payload, but were not observed. More specifically, a ~ 2.2 micron band associated with Al-OH in clay minerals such as illite and Al smectite (and/or hydrated silica) was not observed in any target from Hogwallow Flats or Yori Pass. The high sensitivity of the SuperCam VISIR technique to Al clay minerals such as illite suggests either it is absent or below the detection limit of this technique (e.g., 1–5 wt. %, Mandon et al., 2022). However, quantitative x-ray diffraction and thin section analysis are both needed to confirm the absence of illite from drilled samples.

While it is clear that Gale crater has experienced episodes of burial and erosion, and could have once been much more filled, there is no evidence for comparatively deep burial of sediments in Jezero crater. It is likely that the emplacement of the Jezero sedimentary fan (Figure 1) represents the last major episode of sedimentation into Jezero crater; thus, rocks of the Shenandoah formation perhaps were never deeply buried. Previous work by Quantin-Nataf et al. (2023) on the exhumation history of the crater floor unit (underlying the Shenandoah formation) indicated a shallow burial depth of ~ 40 m. The Jezero fan itself is eroding, but in its core are inverted boulder-rich channels, of which the total thickness from the base of the delta to the boulder-rich channels is only a few tens of meters (Quantin-Nataf et al., 2023). Compared to the crater floor, the Hogwallow Flats member represents the uppermost portion of the Shenandoah formation (Figure 5) so even shallower depths of burial are possible than those of the crater floor (a maximum of tens of meters). Our interpretations of relatively minimal late diagenesis support these predictions of shallow depths of burial.

5.1.5. Origin of Fe/Mg Sulfates

Early diagenesis could also have produced the bedrock Fe/Mg sulfate enrichment observed in Facies 1. A model in which anoxic saline brines interacted with detrital sediments is consistent with the observed textures and mineralogy, including small veinlets and bedrock sulfate cement. Sulfate-cemented outcrop on Earth can indicate primary deposition and cementation under arid and/or hypersaline conditions (Amundson et al., 2008; Benison & Laclair, 2003; Kelts & Shahrabi, 1986). These syndepositional fine-grained sulfate minerals could have precipitated from hypersaline fluids under anoxic conditions (Kelts & Shahrabi, 1986; Pontefract et al., 2017). Sulfate enrichments were not observed in the form of ubiquitous beds of pure sulfates (e.g., cumulate crystals) or lake bottom-growth deposits (Rapin et al., 2019). Episodic saturation by sulfate-rich brines may have led to precipitation of Mg and Fe sulfate within sediments, either in subaerial (evaporative enrichment and/or repeated wet/dry cycles), or subaqueous settings (downward diffusion of supersaturated brines) (Achilles et al., 2020; Chipera et al., 2023; Rapin et al., 2019). This is evidenced by petrographic-scale observations of Yori Pass member bedrock showing multiple generations of sulfates of both detrital and authigenic origin (Benison et al., 2024). Fe/Mg sulfate enrichment within beds of large lateral extent as inferred for the Hogwallow Flats member therefore points toward widespread syndepositional/early diagenesis of sediments in Jezero crater. For the origin of Fe/Mg sulfate to be explained by a later alteration event, such a fluid would have to be extremely concentrated in sulfate to cement sediments with the ~ 20 wt. % Fe/Mg sulfate seen throughout the facies. Such an extreme late diagenetic fluid composition is perhaps less likely than direct precipitation from a hypersaline lake setting.

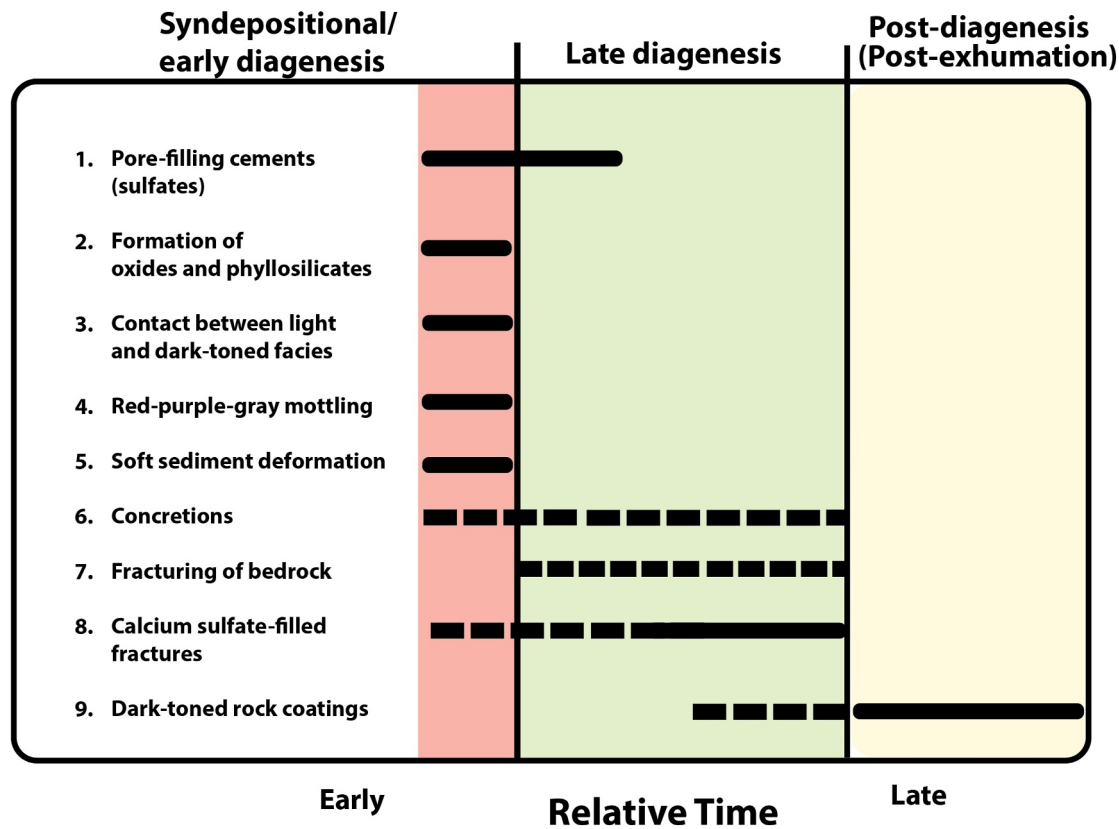


Figure 16. Sequence of alteration events proposed for the Hogwallow Flats/Yori Pass members based on diagenetic features and textures observed by Perseverance.

5.2. Reconstructing Alteration History

We used all the observations described previously to propose a history of diagenesis for the Hogwallow Flats and Yori Pass members (Figure 16). Features that may have resulted from syndepositional or early diagenetic processes include pore-filling sulfate cements, the red-purple-gray mottling, and the formation of concretions. Fracturing may have occurred at any time (either early or late), and the same could be the case for the precipitation of sulfate within these fractures. Ca-sulfate-filled fractures cutting through unfilled (empty) networks of polygonal fractures suggest either multiple episodes of fracturing and fluid flow, or preferential fill of some fractures during or after fracturing occurred. Dark-toned rock coatings likely formed after exhumation, indicating these represent the youngest of the alteration features observed throughout the Hogwallow Flats/Yori Pass members.

Two endmember hypotheses are proposed to explain the formation of diagenetic features, based on the two possible depositional environments (Figure 17). In the alluvial floodplain model, detrital Fe/Mg phyllosilicate-rich sediments were deposited (e.g., sourced from the watershed) in overbank settings and were subsequently chemically altered after deposition (e.g., syndepositional or early diagenetic) by meteoric waters and/or groundwater. In the lacustrine/prodeltaic model, subaqueous deposition of these sediments was followed by chemical alteration in a saline, redox-stratified lake (e.g., Hurowitz et al., 2017). In both cases, a circumneutral pH of alteration fluids may have been followed by acidic pH of alteration fluids (Hurowitz et al., 2023). Both scenarios are consistent with a sedimentary sequence represented by laterally extensive, fine-grained, horizontally laminated sandstones and mudstones (Stack et al., 2024).

The available sedimentological evidence cannot currently distinguish between the two depositional hypotheses (e.g., subaerial floodplain vs. lacustrine/prodeltaic), because sedimentary features of these environments are non-unique (Stack et al., 2024). As such, we leave open the possibility for either case to have occurred. In both situations, we favor the hypothesis that detrital Fe/Mg clays and detrital sulfates were deposited first (Figure 17). A

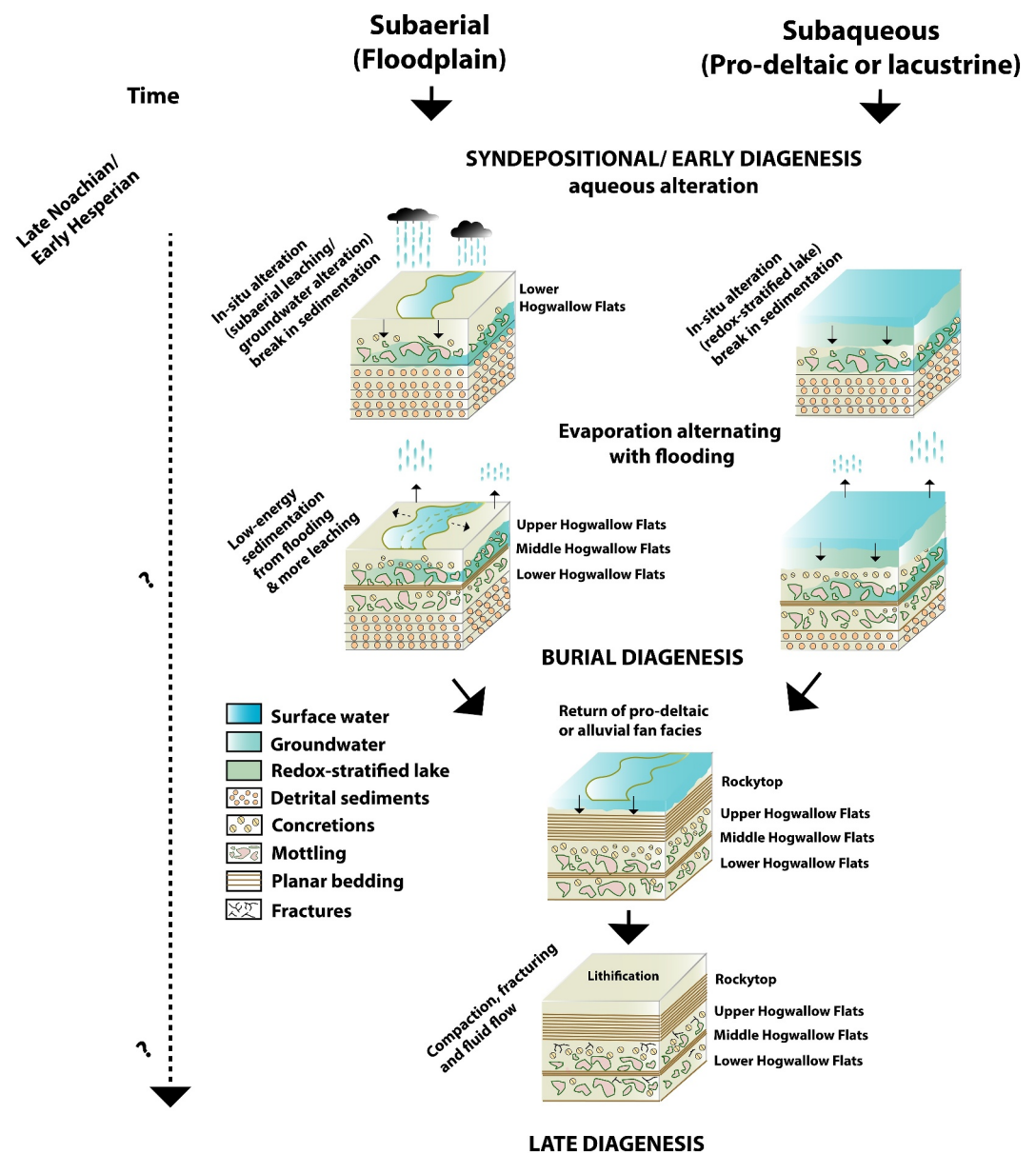


Figure 17. Conceptual diagram outlining the depositional and diagenetic history of the Hogwallow Flats and Yori Pass members of the Shenandoah formation. This scenario considers either deposition in a subaerial (left) or a lacustrine/prodeltaic environment (right), followed by in situ chemical alteration during a break in sedimentation, then returning to a period of low-energy sedimentation and additional in situ chemical alteration. Burial diagenesis began during a return of pro-deltaic or alluvial fan facies, later followed by compaction, additional fracturing and fluid flow.

hybrid model is also possible, in which the sediments were deposited in a subaqueous setting but were later leached in subaerial or shallow subsurface settings due to a decrease in base level.

To link diagenetic features/textures with the alteration model above, we propose the following sequence of events, outlined for each of the two depositional scenarios (Figure 17). Deposition of sulfate-rich detrital sediments in alluvial floodplain settings (left) or pro-deltaic/lacustrine settings (right) was followed by syndepositional/early diagenetic in situ chemical alteration that formed mottling features and concretions in the lower Hogwallow Flats sub-member; a subsequent return in low-energy sedimentation (either from bank flooding, [left], or progradation of delta/lacustrine [right]) and additional chemical alteration of new protolith (Middle Hogwallow Flats, Facies 3) under variable redox conditions again formed mottling features and abundant concretions in the upper Hogwallow Flats member. Subsequent burial by tens of meters of overburden from a return

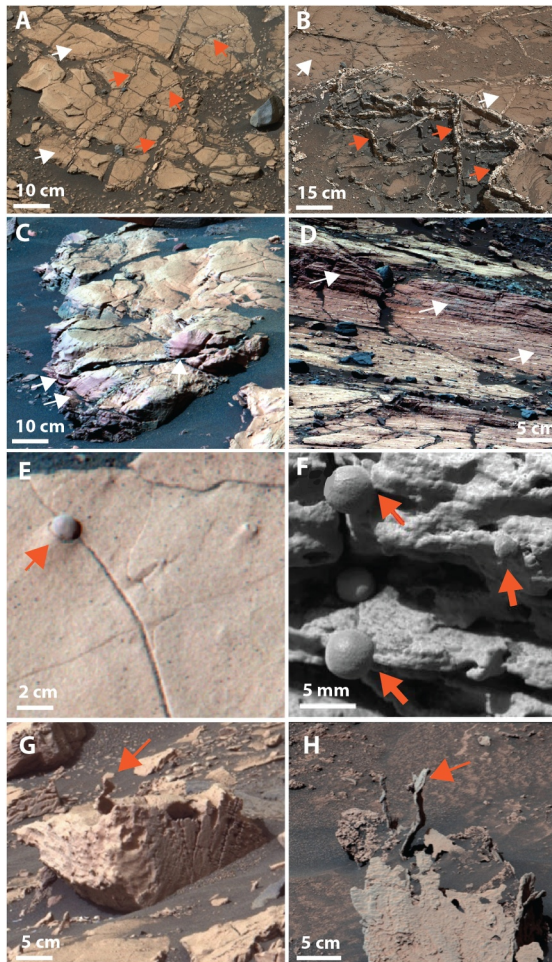


Figure 18. Diagenetic features and textures at the Hogwallow Flats member of the Shenandoah formation, Jezero Crater, Mars (left column) compared to previous observations at Gale and Victoria Craters, Mars (right column). (a) Ca-sulfate -filled fractures (red arrows) at Hidden Harbor, Yori Pass, Jezero Crater (zcam 08621, Sol 614); (b) Anhydrite fracture fill (red arrows) at Garden City, Murray formation, Gale Crater, mcam 04150, Sol 944 (Kronyak et al., 2019); (c) and (d) red-toned bedrock (white arrows) at Piney Ridge, Hogwallow Flats member, Jezero Crater (“c,” zcam 03418, Sol 524) and Jemtland outcrop, Sutton Island member of the Murray formation, Gale Crater (“d,” mcam 08215, Sol 1608); (e) and (f) Fe-oxide bearing concretions (red arrows) in bedrock at Pignut Mountain outcrop, Hogwallow Flats, Jezero Crater (“e,” zcam 03378, Sol 524) and Last Chance outcrop, Burns formation, Eagle Crater, Meridiani Planum (MicroImager, Sol 39); (g) and (h) Putative fracture fill in light-toned bedrock (red arrows) at upper Hogwallow Flats sub-member, Jezero Crater (“g,” zcam 08487, Sol 467) and at the sulfate-bearing unit, Gale Crater (Sol 3424).

of pro-deltaic or alluvial fan facies (lower Rockytop) marked the beginning of burial diagenesis (compaction, lithification, fracturing, and fluid flow).

In either case, burial diagenesis began after deposition of overlying coarse-grained sandstones of lower Rocky Top (Hogwallow flats member and Whale Mountain (Yori Pass member) and was followed by lithification and fracturing. Later diagenetic fluid flow in either scenario is indicated by occasional cm-scale, Ca sulfate-filled fractures, but extensive networks of filled fractures that cross cut stratigraphy were not observed (Figure 17). The development of Mn-rich rock coatings represents recent weathering of outcrop surfaces after deflation-driven exhumation of the western Jezero delta.

5.3. Comparisons With Other Locations on Mars

Diagenetic features and textures observed at Jezero crater are similar to those observed by current and past rover missions on Mars (Figure 18). Comparisons with past observations can provide context for new observations at Jezero. Many of the features are unique within the context of Jezero crater, thus requiring comparisons to other studies on Mars. Features interpreted here as resulting from diagenesis, such as the formation of sulfate cements in Facies 2 and the red-purple-gray colors in Facies 1, have been observed elsewhere on Mars. These include mottling, red-toned bedrock, mineral-filled fractures, and concretions have been previously observed at Gale Crater (Haber et al., 2022; Horgan et al., 2019; Kronyak et al., 2019; Stack et al., 2014; Sun et al., 2019) and Meridiani Planum (McLennan et al., 2005; Morris et al., 2006; Squyres et al., 2004) (Figure 18).

Sulfate-enriched bedrock has been previously observed at Victoria crater (Squyres et al., 2004) as part of the Burns formation (McLennan et al., 2005) at Meridiani Planum. Sulfate enrichment and the formation of concretions in eolian sandstones of the Burns formation is inferred to have occurred in an arid/hyperarid setting (e.g., playa lake) that alternated with fluvial/lacustrine conditions (Hayes et al., 2011; McLennan et al., 2005). Upward evaporation of groundwater may have formed sulfates in the Burns formation strata (McLennan et al., 2005). Alternatively, downward percolation of acidic and sulfur-rich meteoritic water over thousands of years (e.g., pedogenic alteration) may have also contributed to chemical alteration of the Burns formation under predominantly hyperarid conditions, with repeating wet-dry cycles forming desiccation features and eventually soil structure (Amundson, 2018; Rapin et al., 2023). In either case, bedrock sulfate enrichment at Victoria crater was likely an early diagenetic feature, whereas the formation of cross cutting fractures and vein fill likely represents late diagenesis.

Red-toned bedrock and putative mottling features were also observed in the Murray formation (Sol ~1500) and the Carolyn Shoemaker formation (Sol ~1900) (Haber et al., 2022; Horgan et al., 2019; Sun et al., 2019). The presence of these features, along with abundant Mg sulfate and Fe/Mg

phyllosilicates, suggests the Hogwallow Flats member may be more analogous to some intervals of the Murray formation, such as the Sutton Island member (Rampe et al., 2020; Thorpe et al., 2022), but detailed geochemical/mineralogical comparisons are needed to support this hypothesis (e.g., Frydenvang et al., 2020). In any case, it is possible that the Hogwallow Flats member experienced relatively similar early diagenetic alteration as inferred for select intervals of Gale crater strata, such as open-system alteration with liquid water at circumneutral to acidic pH (Mangold et al., 2019; Turner et al., 2021), which in the case of the Sutton Island member of the Murray formation possibly included periods of leaching and pedogenesis in a lake margin paleoenvironment (Gwizd et al., 2024; Haber et al., 2022).

Mottling features and red-toned bedrock observed at the Hogwallow Flats and Yori Pass members are also similar to features observed in the Sutton Island Member of the Murray formation. The formation of the mottling and red-toned bedrock has been inferred to result from open-system leaching under variable redox conditions in lake-margin settings (Gwizd et al., 2024; Haber et al., 2022). Ponding water or anoxic conditions likely resulted in the formation of redox gradients, which indicate habitable environments (Hurowitz et al., 2017) and enhanced preservation of organic matter and other biosignatures (Boye et al., 2017; Hays et al., 2017; Hedges & Keil, 1995).

Other red-gray mottling features on Mars have been attributed to substantial late diagenesis, such as the gray patches alternating with red-toned bedrock outcrops at Vera Rubin Ridge, Gale Crater. These prominent red-gray mottling features consist of large patches (1–10 m) of coarse-grained gray hematite containing mm-scale, dark-toned Fe^{3+} -rich nodules, as well as extensive vein networks that crosscut stratigraphy (Fraeman et al., 2020). These do not as closely resemble mottling features at Hogwallow Flats in scale or composition. Unlike the large-scale (~1–10 m) mottles of patchy gray hematite of late diagenetic origin at Vera Rubin Ridge, mottling features throughout the Hogwallow Flats and Yori Pass members tended to occur at the centimeter to decimeter scales. Furthermore, there were no dark, mm-scale Fe^{3+} -rich nodular features, unlike Vera Rubin ridge where small, nearly pure Fe oxide nodules are associated with gray hematite patches (Fraeman et al., 2020).

Concentric and hollow concretions (Kalucha et al., 2024) are also similar to those observed in the Murray formation (Karasburg and Sutton Island Members) (Sun et al., 2019). Some of the concretions appeared hollow and/or filled, similar to hollow concretions interpreted as early diagenetic from Yellowknife Bay, Gale crater (Stack et al., 2014). The Fe-oxide enriched “blueberries” observed by Opportunity at Victoria crater also resemble some of the Fe-oxide bearing concretions observed at the Pignut Mountain outcrop, Hogwallow Flats member (Figure S6 in Supporting Information S1). However, there are notable differences in scale, abundance, and distribution: concretions at Jezero have not been observed as abundant float or forming carpets of lag deposits, unlike those at Victoria crater (Squyres et al., 2004).

5.4. Implications for Biosignature Preservation Potential

In the context of biosignature preservation, a key finding of this work is that *Perseverance* may have collected core samples into the dark-toned, mottled and potentially less oxidized facies (Facies 1) that lies directly below the light-toned, laminated to massive mudstones of Facies 2, both at the Hogwallow Flats and Yori Pass members (Figure 19). As a result, it is possible that two distinct geochemical environments are represented in each sample core. These may include one of early diagenetic sulfate precipitation (e.g., hypersaline conditions, Facies 2) and one possibly of increased water availability and variable redox state associated with a shallow lake or alluvial floodplain environment (dark-toned, mottled Facies 1).

While SuperCam visible spectra exhibited a 0.43 micron band associated with ferric sulfates in all abrasion and tailings observations (Figure 14), Mastcam-Z observations suggested limited or altogether absent Fe^{3+} signatures in abrasions and tailings from the Yori Pass member (Figure 13). This suggests the Kukaklek sample could have undergone limited oxidation, and thus may represent some of the least diagenetically altered material from this interval in the Shenandoah formation. Interpretations of limited oxidation of the Yori Pass sample comes primarily from observations of drill core tailings and are centered around three lines of evidence. Firstly, the drill core tailings at Yori Pass resulting from collection of the Kukaklek core are much darker relative to drill tailings at the Hogwallow Flats member (Figure 13). These color differences between the drill tailings are also apparent in Mastcam-Z decorrelation stretches (Figure 12). Color differences could result from photometric effects or homogenization during drilling. However, drill core tailings are distinctly darker than abrasion tailings and appeared to show darker-toned fines excavated from depths of ~6–8 cm during coring. Color differences are unlikely to be due to photometric effects because all multispectral images were taken within 1 hr of local solar noon (Hayes et al., 2021) (Methods). Second, a key difference was that the Kukaklek core tailings lacked the distinct purple color (often associated with Fe^{3+} -bearing material) in the near-infrared DCS (Figure 12) that was observed in the Hazeltop core tailings (Hogwallow Flats), indicating that the tailings are compositionally distinct between the two locations. Lastly, the spectra (Figure 13) and the 528 nm band parameter maps displayed at the same scale (Figure 12) displayed depleted 528 nm band depths in Kukaklek, indicating this sample contained less Fe^{3+} -bearing material relative to Hazeltop. Spectra also exhibited weaker 866 nm bands (Figure 13) consistent with a more limited Fe^{3+} component in Kukaklek. This suggests that the Yori Pass member sample is overall less

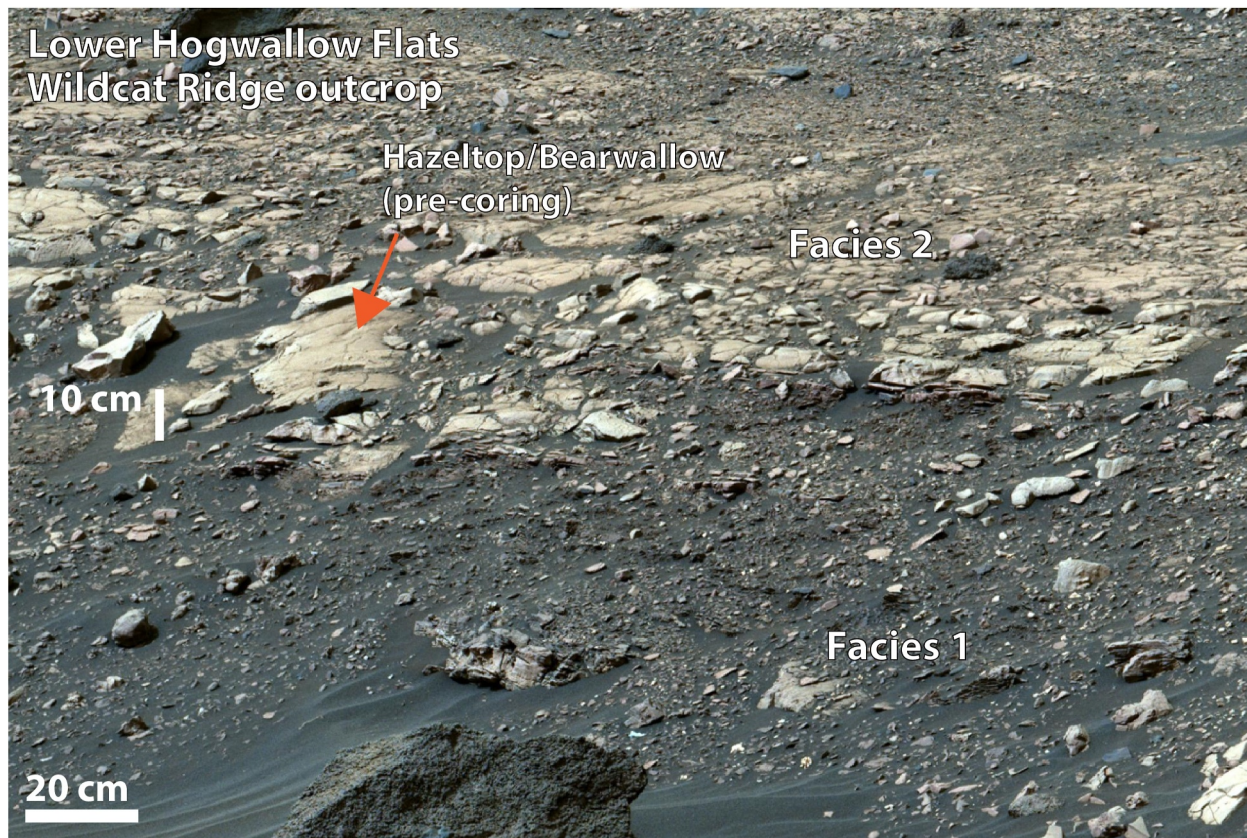


Figure 19. Context for sampling at the Hogwallow Flats member. Facies 1 (dark-toned, mottled) overlain by 10–15 cm of Facies 2 (light-toned) at the lower Hogwallow Flats sub-member showing pre-coring location for Hazeltop/Bearwallow samples (Sol 461, zcam08482; 10 cm scale shown for approximate sampling depth of drilled samples (~4–6 cm).

oxidized, and that the Kukaklek core sample represents some of the least oxidized material encountered throughout this interval of the Shenandoah formation.

One hypothesis for these differences in oxidation state between Yori Pass and Hogwallow Flats is that collection of the drilled sample penetrated through the light-toned Facies 2 (Figure 9) and into the darker toned, mottled bedrock of Facies 1. Of the two, the Kukaklek core was the “short” core of approximately 48.7 mm in length as measured by *Perseverance's* volume probe, whereas the Hazeltop and Bearwallow cores measured 59.7 and 62.4 mm, respectively (Bosak et al., 2024). From outcrop images of wheel-fractured bedrock (Figure 9), it is possible that Facies 2 at Hidden Harbor outcrop was thinner (~2–5 cm) than at Wildcat Ridge where it appears to be ~10–15 cm thick (Figure 19), so it is plausible that the “short” Kukaklek core could have more easily penetrated into Facies 1.

The three rock cores collected from the Hogwallow Flats and Yori Pass members, Hazeltop, Bearwallow and Kukaklek (Figure 4), may therefore contain material of variable redox state. Of the three, Kukaklek appears distinct with its relative lack of Fe^{3+} -bearing phases. Collection of a potentially less oxidized sample in these cores has major implications for interpretations of climate, habitability, and biosignature preservation potential (Bosak et al., 2024). This sample may have a high organic preservation potential due to the inferred low abundances of Fe^{3+} phases typically associated with oxidizing conditions that could have destroyed organics associated with clay minerals. Organic matter on Earth is preserved well in anoxic environments, where either fast sedimentation or mineral precipitation reduce microbial activity and the delivery of oxidants that oxidize reduced carbon in organic matter (Hartnett et al., 1998; Hedges & Keil, 1995; McMahon et al., 2018). Terrestrial organics that are associated with partially or strongly reducing conditions before burial tend to be preserved in greater abundances relative to strongly oxidizing conditions before burial (Boye et al., 2017; Hedges & Oades, 1997;

Watanabe et al., 2000). Alternatively, organic matter can be preserved well by entrapment during rapid precipitation of salt minerals, regardless of whether the environment is oxic or anoxic (Benison, 2019).

In addition to potential differences in redox state between upper and lower portions of the outcrops, several additional textural and chemical features of rocks from the Hogwallow Flats member are associated with enhanced biosignature preservation. These include fine-grained textures (fine sandstones/mudstones), the presence of Fe/Mg phyllosilicates (Figure 15), depositional and diagenetic sulfates (Benison et al., 2023, 2024), and a diverse suite of concretions, which could be sites of enhanced organic preservation (Kalucha et al., 2024). Specifically, the Bearwallow core at Hogwallow Flats may have sampled through a putative mm-scale concretion, based on pre-coring images of the Wildcat Ridge outcrop (Figure S10 in Supporting Information S1). Organic matter has a high affinity for sorption to clay minerals (e.g., Fornaro et al., 2018 and references therein), a process that may encourage preservation of organic carbon over geological time scales (Watanabe et al., 2004). Similarly, the presence of sulfates is associated with organic preservation, either via entrapment in fluid inclusions (Benison, 2019; Benison & Karmanocky, 2014) or in the crystal lattice structure of Mg sulfate itself (Benison, 2019; François et al., 2015). Finally, these rocks appear to have undergone only shallow burial by a maximum of tens of meters of sediments (Quantin-Nataf et al., 2023), perhaps minimizing the effects of burial diagenesis while achieving a sufficient depth for insulating sedimentary organics from cosmic-ray induced degradation (e.g., Dartnell et al., 2012).

6. Conclusions

The Hogwallow Flats and Yori Pass members of the Shenandoah formation are composed of between three to ten vertical meters of fine-grained sedimentary rock. The mineralogy and morphology of these rocks are distinct from all other rock units observed in Jezero crater as of mission Sol ~1100.

Building upon the sedimentology and stratigraphy of Stack et al. (2024), we identified three facies of the Hogwallow Flats member at Hawksbill Gap that were deposited in a floodplain or lacustrine/prodeltaic environment. Facies 1 represents the dark-toned, red-green-gray mottled mudstones (inferred grain size). Facies 2 is typified by light-toned, tan colored massive to laminated fine sandstones and mudstones, while Facies 3 consists of low angle cross-stratified sandstones also with inferred grain size. At the Hawksbill Gap East stratigraphic section, we identified three sub-members of the Hogwallow Flats member. The lower Hogwallow Flats sub-member is composed of 30–40 cm of Facies 1 overlain by five to 15 cm of Facies 2. The middle sub-member is composed of ~30 cm of Facies 3, and the upper sub-member, like the lower sub-member, returns to a similar combination of Facies 1 and 2. At the Yori Pass member, Facies 1 and 2 were again identified at the Hidden Harbor outcrop. Long-distance images of the Intricate Bay outcrop again revealed the extensive mottled appearance of Facies 1 that altogether resembled a thicker version (~3 m) of the lower Hogwallow Flats sub-member.

Mastcam-Z multispectral data and SuperCam reflectance spectra of the Hogwallow Flats and Yori Pass members show that these units are spectrally distinct from other units in the Shenandoah formation, and long-distance images reveal that this interval could have once been widely distributed throughout the western Jezero fan. The emplacement and subsequent diagenesis of this interval may represent a widespread habitable lacustrine and/or alluvial floodplain paleoenvironment. Based on observations of diagenetic features and comparisons with Earth analogs, we interpret this interval of the Shenandoah formation as experiencing early diagenesis and mineral precipitation under variable redox conditions and salinity.

Overall, the Hogwallow Flats and Yori Pass members appear to have experienced limited diagenesis. Of the alteration that did occur, we speculate that an early diagenetic origin is plausible for features such as the concretions, the red-purple-gray mottling and Fe/Mg sulfate cements. Evidence of significant late fluid flow, such as extensive filled fractures that cross-cut stratigraphy, were minimal or absent from these intervals of the Shenandoah formation.

Bedrock Mg sulfate enrichment, concretions, and red-purple-gray mottling observed at Hogwallow Flats and Yori Pass are similar to features previously observed at Gale crater and Victoria crater on Mars, though at different scales, abundances and distributions. Bedrock mottling noted in Facies 1 may represent early diagenetic water table variations leading to variable redox conditions in subaerial to shallow subaqueous settings such as lake-margin environments, as envisaged for other settings on Mars. In particular, many of the features observed in

Facies 1 were similar to diagenetic features and textures previously observed at the lake-margin facies of the Sutton Island member of the Murray formation at Gale Crater.

The fine-grained textures of Facies 1 and 2 at the Hogwallow Flats member may have reduced susceptibility to late diagenetic fluid flow, which can be associated with the destruction of biosignatures and oxidation of organic carbon. Compared to the finer grain size of the Hogwallow Flats core samples, the Kukaklek sample represents somewhat of a conundrum with its coarser grain size but more limited Fe³⁺ signatures, indicating less oxidation than would be expected for a comparatively coarse-grained rock. One hypothesis is that the Kukaklek core includes the mottled facies (Facies 1) that lies directly below sulfate-cemented outcrop (Facies 2), which appears to be associated with a more variable Fe³⁺ signature. Both of these facies may be sites of enhanced biosignature preservation potential.

Altogether, these features indicate that rock cores collected from the Hogwallow Flats and Yori Pass members of the Shenandoah formation can be ranked among the highest priority samples for biosignature investigation relative to other samples collected so far by *Perseverance* (as of Sol ~1200). These samples may preserve morphological, textural, chemical and/or isotopic biosignatures if life was ever present in ancient Jezero environments. Cores collected from this interval in the Shenandoah formation therefore represent an ongoing incentive for the fulfillment of MSR.

Data Availability Statement

The data in this study are from the Mastcam-Z, SuperCam, PIXL and SHERLOC/WATSON instruments on the Mars 2020 Rover, as well as data from the HiRISE instrument onboard Mars Reconnaissance Orbiter. All data presented here from Mastcam-Z, SuperCam, SHERLOC/WATSON are available through the Planetary Data System Imaging Node (https://pds-imaging.jpl.nasa.gov/portal/mars2020_mission.html) and GeoSciences Node (<https://pds-geosciences.wustl.edu/missions/mars2020/>). HiRISE data are also included (McEwen, 2007). Software packages used for Mastcam-Z image processing, spectral extraction, and statistical analyses are part of the open source “marslab” suite by Million Concepts, LLC (St. Clair et al., 2022). The SuperCam major element oxide composition (MOC) and all raw data and processed calibrated data files are included in the Planetary Data System.

References

- Achilles, C. N., Rampe, E. B., Downs, R. T., Bristow, T. F., Ming, D. W., Morris, R. V., et al. (2020). Evidence for multiple diagenetic episodes in ancient fluvial-lacustrine sedimentary rocks in Gale crater, Mars. *Journal of Geophysical Research: Planets*, 125(8), e2019JE006295. <https://doi.org/10.1029/2019JE006295>
- Allwood, A. C., Hurowitz, J. A., Clark, B. C., Cinquini, L., Davidoff, S., Denise, R. W., et al. (2020). The PIXL Instrument on the Mars 2020 Perseverance Rover. In *Lunar and Planetary Science Conference* (Vol. 2507, pp. 1–9). <https://doi.org/10.48550/arXiv.2103.07001>
- Amundson, R. (2018). Meteoric water alteration of soil and landscapes at Meridiani Planum, Mars. *Earth and Planetary Science Letters*, 488, 155–167. <https://doi.org/10.1016/j.epsl.2018.02.012>
- Amundson, R., Ewing, S., Dietrich, W., Sutter, B., Owen, J., Chadwick, O., et al. (2008). On the in situ aqueous alteration of soils on Mars. *Geochimica et Cosmochimica Acta*, 72(15), 3845–3864. <https://doi.org/10.1016/j.gca.2008.04.038>
- Barnes, R., Gupta, S., Paar, G., Stack-Morgan, K. M., Horgan, B., Crumpler, L., et al. (2023). Constructing geological cross-sections to constrain the three-dimensional stratigraphic architecture of the Jezero delta front. In *Lunar and Planetary Science Conference* (Vol. 2716, pp. 4–5).
- Beatty, D. W., Grady, M. M., McSween, H. Y., Sefton-Nash, E., Carrier, B., Altieri, F., et al. (2019). The potential science and engineering value of samples delivered to Earth by Mars sample return. *Meteoritics & Planetary Sciences*, 67(3), 667–671. <https://doi.org/10.1111/maps.13232>
- Bell, J. F., Maki, J. N., Alwmark, S., Ehlmann, B. L., Fagents, S. A., Grotzinger, J. P., et al. (2022). Geological, multispectral, and meteorological imaging results from the Mars 2020 Perseverance rover in Jezero crater. *Science Advances*, 8(47), eabo4856. <https://doi.org/10.1126/sciadv.abo4856>
- Bell, J. F., Maki, J. N., Mehall, G. L., Ravine, M. A., Caplinger, M. A., Bailey, Z. J., et al. (2021). The Mars 2020 Perseverance Rover Mast Camera Zoom (Mastcam-Z) Multispectral, Stereoscopic Imaging Investigation. *Space Science Reviews*, 217(1), 24. <https://doi.org/10.1007/s11214-020-00755-x>
- Benison, K. C. (2019). How to search for life in Martian chemical sediments and their fluid and solid inclusions using petrography and spectroscopic methods. *Frontiers in Environmental Science*, 7, 108. <https://doi.org/10.3389/fenvs.2019.00108>
- Benison, K. C., Bosak, T., Clark, B., Czaja, A. D., Fornaro, T., Gill, K., et al. (2023). Biosignature potential and possible environmental indicators of sulfate-rich rocks from Hogwallow Flats and Yori Pass, Jezero Crater Delta Front, Mars. In *Lunar and Planetary Science Conference* (Vol. 2023, pp. 6–7).
- Benison, K. C., Gill, K. K., Sharma, S., Siljeström, S., Zawaski, M., Bosak, T., et al. (2024). Depositional and diagenetic sulfates of Hogwallow Flats and Yori Pass, Jezero crater: Evaluating preservation potential of environmental indicators and possible biosignatures from past Martian surface waters and groundwaters. *Journal of Geophysical Research: Planets*, 129(2), e2023JE008155. <https://doi.org/10.1029/2023JE008155>
- Benison, K. C., & Karmanocky, F. J. (2014). Could microorganisms be preserved in Mars gypsum? Insights from terrestrial examples. *Geology*, 42(7), 615–617. <https://doi.org/10.1130/G35542.1>

Acknowledgments

The authors acknowledge the immense efforts of the Mars 2020 science and engineering teams for the completion of this work. Contributions from four anonymous reviewers greatly improved the manuscript.

- Benison, K. C., & Laclair, D. A. (2003). Modern and ancient extremely acid saline deposits: Terrestrial analogs for Martian environments? *Astrobiology*, 3, 609–618. <https://doi.org/10.1089/153110703322610690>
- Bhartia, R., Beegle, L. W., DeFlores, L., Abbey, W., Razzell Hollis, J., Uckert, K., et al. (2021). Perseverance's scanning habitable environments with Raman and luminescence for organics and chemicals (SHERLOC) investigation. *Space Science Reviews*, 217(4), 58. <https://doi.org/10.1007/s11214-021-00812-z>
- Blodgett, R. H., Crabaugh, J. P., & McBride, E. F. (1993). The color of red beds—A geologic perspective. *Soil Color*, 31, 127–159. <https://doi.org/10.2136/sssaspepub31.c8>
- Bosak, T., Shuster, D. L., Scheller, E. L., Siljeström, S., Zawaski, M. J., Mandon, L., et al. (2024). Astrobiological potential of rocks acquired by the Perseverance rover at a sedimentary fan front in Jezero crater, Mars. *AGU Advances*, 5(4), e2024AV001241. <https://doi.org/10.1029/2024AV001241>
- Boye, K., Noël, V., Tfaily, M. M., Bone, S. E., Williams, K. H., Bargar, J. R., & Fendorf, S. (2017). Thermodynamically controlled preservation of organic carbon in floodplains. *Nature Geoscience*, 10(6), 415–419. <https://doi.org/10.1038/ngeo2940>
- Bristow, T. F., Grotzinger, J. P., Rampe, E. B., Cuadros, J., Chipera, S. J., Downs, G. W., et al. (2021). Brine-driven destruction of clay minerals in Gale crater, Mars. *Science*, 373(6551), 198–204. <https://doi.org/10.1126/science.abg5449>
- Broz, A. P., Horgan, B. H. N., Kalucha, H., Johnson, J. R., Royer, C., Dehouck, E., et al. (2024). Biosignature preservation potential of sulfate-rich rocks from Hogwallow Flats, Jezero Crater, Mars. In *Lunar and Planetary Science Conference* (Vol. 1259, pp. 10–11).
- Burns, R. (1993). *Mineralogical applications of crystal field theory*. Cambridge University Press.
- Chan, M. A., & Parry, W. T. (2000). Diagenetic hematite and manganese oxides and fault-related fluid flow in Jurassic sandstones of southeastern Utah. *AAPG Bulletin*, 84, 1281–1310. <https://doi.org/10.1306/a9673e82-1738-11d7-8645000102c1865d>
- Chipera, S. J., Vaniman, D. T., Rampe, E. B., Bristow, T. F., Martínez, G., Tu, V. M., et al. (2023). Mineralogical investigation of Mg-sulfate at the Canaima drill site, Gale crater, Mars. *Journal of Geophysical Research: Planets*, 128(11), e2023JE008041. <https://doi.org/10.1029/2023JE008041>
- Combe, J. P., Le Mouélic, S., Sotin, C., Gendrin, A., Mustard, J., Le Deit, L., et al. (2008). Analysis of OMEGA/Mars Express data hyperspectral data using a Multiple-Endmember Linear Spectral Unmixing Model (MELSUM): Methodology and first results. *Planetary and Space Science*, 56(7), 951–975. <https://doi.org/10.1016/j.pss.2007.12.007>
- Cornell, R. M., & Schwertmann, U. (2003). *The iron oxides: Structure, properties, reactions, occurrences and uses*. Wiley-VCH. <https://doi.org/10.1002/3527602097>
- Dartnell, L. R., Page, K., Jorge-villar, S. E., Wright, G., Munshi, T., Scowen, I. J., et al. (2012). Destruction of Raman biosignatures by ionising radiation and the implications for life detection on Mars. *Analytical and Bioanalytical Chemistry*, 403(1), 131–144. <https://doi.org/10.1007/s00216-012-5829-6>
- Dehouck, E., Forni, O., Quantin-Nataf, C., Beck, P., Mangold, N., Royer, C., et al. (2023). Overview of the bedrock geochemistry and mineralogy observed by Supercam during Perseverance's delta front campaign. In *Lunar and Planetary Science Conference* (Vol. 2862, pp. 31–41).
- Driese, S. G., Medaris, L. G., Kirsimäe, K., Somelar, P., & Stinchcomb, G. E. (2018). Oxisol processes and geochemical constraints on duration of weathering for Neoproterozoic Baltic paleosol. *Precambrian Research*, 310, 165–178. <https://doi.org/10.1016/j.precamres.2018.02.020>
- Driese, S. G., Simpson, E. L., Eriksson, K. A., & Block, E. (1995). Redoximorphic paleosols in alluvial and lacustrine deposits, 1.8 Ga Lochness Formation, Mount Isa, Australia: Pedogenic processes and implications for paleoclimate. *Journal of Sedimentary Research*, 65(4a), 675–679. <https://doi.org/10.1306/d4268199-2b26-11d7-8648000102c1865d>
- Eichhubl, P., Taylor, W. L., Pollard, D. D., & Aydin, A. (2004). Paleo-fluid flow and deformation in the Aztec Sandstone at the Valley of Fire, Nevada—Evidence for the coupling of hydrogeologic, diagenetic, and tectonic processes. *Bulletin of the Geological Society of America*, 116(9–10), 1120–1136. <https://doi.org/10.1130/B25446.1>
- Farley, K. A., Stack, K. M., Shuster, D. L., Horgan, B. H. N., Hurowitz, J. A., Tarnas, J. D., et al. (2022). Aqueously altered igneous rocks sampled on the floor of Jezero crater, Mars. *Science*, 377(6614), eabo2196. <https://doi.org/10.1126/science.abo2196>
- Farley, K. A., Williford, K. H., Stack, K. M., Bhartia, R., Chen, A., de la Torre, M., et al. (2020). Mars 2020 Mission Overview. *Space Science Reviews*, 216(8), 142. <https://doi.org/10.1007/s11214-020-00762-y>
- Fassett, C. I., & Head, J. W. (2005). Fluvial sedimentary deposits on Mars: Ancient deltas in a crater lake in the Nili Fossae region. *Geophysical Research Letters*, 32(14), L14201. <https://doi.org/10.1029/2005GL023456>
- Ferguson, R., Hare, T., Mayer, D., Galuszka, D., Redding, B., Smith, E., et al. (2020). Mars 2020 Terrain Relative Navigation Flight Product Generation: DTM and Orthorectified Image Mosaics. In *Lunar and Planetary Science Conference* (Vol. 21, pp. 1–9).
- Fornaro, T., Steele, A., & Brucato, J. R. (2018). Catalytic/protective properties of martian minerals and implications for possible origin of life on Mars. *Life*, 8(4), 1–41. <https://doi.org/10.3390/life8040056>
- Fouchet, T., Reess, J. M., Montmessin, F., Hassen-Khodja, R., Nguyen-Tuong, N., Humeau, O., et al. (2022). The SuperCam infrared spectrometer for the perseverance rover of the Mars2020 mission. *Icarus*, 373, 114773. <https://doi.org/10.1016/j.icarus.2021.114773>
- Fraeman, A. A., Edgar, L. A., Rampe, E. B., Thompson, L. M., Frydenvang, J., Fedo, C. M., et al. (2020). Evidence for a Diagenetic Origin of Vera Rubin Ridge, Gale Crater, Mars: Summary and Synthesis of Curiosity's Exploration Campaign. *Journal of Geophysical Research: Planets*, 125(12), e2020JE006527. <https://doi.org/10.1029/2020JE006527>
- François, P., Szopa, C., Buch, A., Coll, P., Mccadam, A. C., Mahaffy, P. R., et al. (2015). Magnesium sulfate as a key mineral for the detection of organic molecules on Mars using pyrolysis. *Journal of Geophysical Research: Planets*, 121(1), 61–74. <https://doi.org/10.1002/2015JE004884>
- Frydenvang, J., Mangold, N., Wiens, R. C., Fraeman, A. A., Edgar, L. A., Fedo, C. M., et al. (2020). The chemostratigraphy of the Murray formation and role of diagenesis at Vera Rubin Ridge in Gale Crater, Mars, as observed by the ChemCam Instrument. *Journal of Geophysical Research: Planets*, 125(9), e2019JE006320. <https://doi.org/10.1029/2019JE006320>
- Gerhard, E. (2000). *Sedimentary basins—Evolution, facies and sediment budget* (p. 792). Springer-Verlag.
- Goudge, T. A., Mohrig, D., Cardenas, B. T., Hughes, C. M., & Fassett, C. I. (2018). Stratigraphy and paleohydrology of delta channel deposits, Jezero crater, Mars. *Icarus*, 301, 58–75. <https://doi.org/10.1016/j.icarus.2017.09.034>
- Gwizd, S., Fedo, C., Grotzinger, J., Banham, S., Rivera-Hernández, F., Gupta, S., et al. (2024). Evolution of a lake margin recorded in the Sutton Island member of the Murray formation, Gale crater, Mars. *Journal of Geophysical Research: Planets*, 129(1), e2023JE007919. <https://doi.org/10.1029/2023JE007919>
- Haber, J. T., Horgan, B., Fraeman, A. A., Johnson, J. R., Wellington, D., Cloutis, E., et al. (2022). Mineralogy of a possible ancient lakeshore in the Sutton Island member of Mt. Sharp, Gale crater, Mars, from Mastcam multispectral images. *Journal of Geophysical Research: Planets*, 127(10), e2022JE007357. <https://doi.org/10.1029/2022JE007357>
- Hartnett, H., Keil, R. G., Hedges, J., & Devol, A. H. (1998). Influence of oxygen exposure time on organic carbon preservation in continental margin sediments. *Nature*, 391(6667), 572–575. <https://doi.org/10.1038/35351>

- Hayes, A. G., Corlies, P., Tate, C., Barrington, M., Bell, J. F., Maki, J. N., et al. (2021). Pre-flight calibration of the Mars 2020 Rover Mastcam Zoom (Mastcam-Z) multispectral, stereoscopic imager. *Space Science Reviews*, 217(2), 29. <https://doi.org/10.1007/s11214-021-00795-x>
- Hayes, A. G., Grotzinger, J. P., Edgar, L. A., Squyres, S. W., Watters, W. A., & Sohl-Dickstein, J. (2011). Reconstruction of eolian bed forms and paleocurrents from cross-bedded strata at Victoria Crater, Meridiani Planum, Mars. *Journal of Geophysical Research*, 116, E00F21. <https://doi.org/10.1029/2010JE003688>
- Hays, L. E., Graham, H. V., Des Marais, D. J., Hausrath, E. M., Horgan, B., McCollom, T. M., et al. (2017). Biosignature preservation and detection in Mars analog environments. *Astrobiology*, 17(4), 363–400. <https://doi.org/10.1089/ast.2016.1627>
- Hedges, J., & Keil, R. G. (1995). Sedimentary organic matter preservation: An assessment and speculative synthesis. *Marine Chemistry*, 49(2–3), 123–126. [https://doi.org/10.1016/0304-4203\(95\)00011-F](https://doi.org/10.1016/0304-4203(95)00011-F)
- Hedges, J. I., & Oades, J. M. (1997). Comparative organic geochemistries of soils and marine sediments. *Organic Geochemistry*, 27(7–8), 319–361. [https://doi.org/10.1016/s0146-6380\(97\)00056-9](https://doi.org/10.1016/s0146-6380(97)00056-9)
- Horgan, B., Udry, A., Rice, M., Alwmark, S., Amundsen, H. E. F., Bell, J. F., III, et al. (2023). Mineralogy, morphology, and emplacement history of the Maaz formation on the Jezero crater floor from orbital and rover observations. *Journal of Geophysical Research: Planets*, 128(8), e2022JE007612. <https://doi.org/10.1029/2022JE007612>
- Horgan, B. H. N., Johnson, J., Fraeman, A., Rice, M. S., Seeger, C., Bell, III, J. F., et al. (2019). Diagenesis of Vera Rubin ridge, Gale crater, Mars from Mastcam multispectral images. *Journal of Geophysical Research: Planets*, 125(11), e2019JE006322. <https://doi.org/10.1002/essoar.10501380.1>
- Hurowitz, J. A., Grotzinger, J. P., Fischer, W. W., McLennan, S. M., Milliken, R. E., Stein, N., et al. (2017). Redox stratification of an ancient lake in Gale crater, Mars. *Science*, 356(6341), eaah6849. <https://doi.org/10.1126/science.aah6849>
- Hurowitz, J. A., Tice, M. M., Allwood, A. C., Cable, M. L., Bosak, T., Broz, A., et al. (2023). The Petrogenetic History of the Jezero Crater Delta Front From Microscale Observations by the Mars 2020 PIXL Instrument. In *Lunar and Planetary Science Conference* (Vol. 2023, pp. 4–5).
- Johnson, J. R., Bell, J. F., Merusi, M., Joseph, J., Rice, M., Dufлот, L., et al. (2023). Recent Spectrophotometric observations along the MSL and Mars 2020 Rover traverses. In *Lunar and Planetary Science Conference* (Vol. 1387, pp. 2022–2023).
- Johnson, J. R., Wiens, R. C., Cloutis, E. A., Mandon, L., Maurice, S., & Legett, C. (2023). Ferric Sulfates at the Jezero Crater Delta Front as Evidenced by SuperCam 433 nm absorptions. In *Lunar and Planetary Science Conference* (pp. 6–7).
- Kalucha, H., Broz, A., Randazzo, N., Aramendia, J., Madariaga, J. M., Garczynski, B., et al. (2024). Probable concretions observed in the Shenandoah Formation of Jezero Crater, Mars and comparison with terrestrial analogs. *Journal of Geophysical Research: Planets*, 129(8), e2023JE008138. <https://doi.org/10.1029/2023JE008138>
- Kelts, K., & Shahrabi, M. (1986). Holocene sedimentology of hypersaline Lake Urima, northwestern Iran. *Palaeogeography, Palaeoclimatology, Palaeoecology*, 54(1–4), 105–130. [https://doi.org/10.1016/0031-0182\(86\)90120-3](https://doi.org/10.1016/0031-0182(86)90120-3)
- Kraus, M. J., & Aslan, A. (1993). Eocene hydromorphic paleosols: Significance for interpreting ancient floodplain processes. *Journal of Sedimentary Petrology*, 63, 453–463. <https://doi.org/10.1306/D4267B22-2B26-11D7-8648000102C1865D>
- Kronyak, R. E., Kah, L. C., Edgett, K. S., VanBommel, S. J., Thompson, L. M., Wiens, R. C., et al. (2019). Mineral-filled fractures as indicators of multigenerational fluid flow in the Pahrump Hills member of the Murray formation, Gale crater, Mars. *Earth and Space Science*, 6(2), 238–265. <https://doi.org/10.1029/2018EA000482>
- Lanza, N., Gasda, P., Ollila, A., Chide, B., Garczynski, B., Johnson, J., et al. (2023). A varnish-like high-manganese rock coating in Jezero crater, Mars. In *EGU General Assembly 2023, Vienna, Austria, 24–28 April 2023* (pp. EGU23–10757). <https://doi.org/10.5194/egusphere-egu23-10757>
- Lepre, C. J., & Olsen, P. E. (2021). Hematite reconstruction of Late Triassic hydroclimate over the Colorado Plateau. *Proceedings of the National Academy of Sciences of the United States of America*, 118(7), e2004343118. <https://doi.org/10.1073/pnas.2004343118>
- Lesh, C., Ives, L. R. W., & Stack, K. M. (2023). Characterization of soft sediment deformation within the Hogwallow Flats member, Shenandoah formation, Jezero crater, Mars. In *AGU Fall Meeting* (Vol. 3231).
- Lopez-Reyes, G., Nachon, M., Veneranda, M., Beyssac, O., Madariaga, J. M., Manrique, J. A., et al. (2023). Anhydrite detections by Raman spectroscopy with SuperCam at the Jezero Delta, Mars. In *Lunar and Planetary Science Conference* (pp. 4–5).
- Maki, J. N., Gruel, D., McKinney, C., Ravine, M. A., Morales, M., Lee, D., et al. (2020). The Mars 2020 Engineering Cameras and microphone on the perseverance rover: A next-generation imaging system for Mars exploration. *Space Science Reviews*, 216(8), 137. <https://doi.org/10.1007/s11214-020-00765-9>
- Mandon, L., Beck, P., Quantin-Nataf, C., Dehouck, E., Thollot, P., Loizeau, D., & Volat, M. (2022). ROMA: A database of rock reflectance spectra for Martian in situ exploration. *Earth and Space Science*, 9(1), e2021EA001871. <https://doi.org/10.1029/2021EA001871>
- Mandon, L., Ehlmann, B. L., Wiens, R. C., Garczynski, B. J., Horgan, B. H. N., Fouchet, T., et al. (2024). Variable iron mineralogy and redox conditions recorded in ancient rocks measured by in situ visible/near-infrared spectroscopy at Jezero crater, Mars. *Journal of Geophysical Research: Planets*, 129(7), e2023JE008254. <https://doi.org/10.1029/2023JE008254>
- Mandon, L., Quantin-Nataf, C., Thollot, P., Mangold, N., Lozac'h, L., Dromart, G., et al. (2020). Refining the age, emplacement and alteration scenarios of the olivine-rich unit in the Nili Fossae region, Mars. *Icarus*, 336, 113436. <https://doi.org/10.1016/j.icarus.2019.113436>
- Mangold, N., Dehouck, E., Fedo, C., Forni, O., Achilles, C., Bristow, T., et al. (2019). Chemical alteration of fine-grained sedimentary rocks at Gale crater. *Icarus*, 321, 619–631. <https://doi.org/10.1016/j.icarus.2018.11.004>
- Mangold, N., Gupta, S., Gasnault, O., Dromart, G., Tarnas, J. D., Sholes, S. F., et al. (2021). Perseverance rover reveals an ancient delta-lake system and flood deposits at Jezero crater, Mars. *Science*, 374(6568), 711–717. <https://doi.org/10.1126/science.abl4051>
- Maurice, S., Wiens, R. C., Bernardi, P., Caïs, P., Robinson, S., Nelson, T., et al. (2021). The SuperCam instrument suite on the Mars 2020 rover: Science objectives and mast-unit description. *Space Science Reviews*, 217(3), 47. <https://doi.org/10.1007/s11214-021-00807-w>
- McEwen, A. S. (2007). MRO Mars high-resolution imaging science experiment, reduced data record V1.1, MRO-M-HIRISE-3-RDR-V1.1 [Dataset]. *NASA Planetary Data System*. <https://doi.org/10.17189/1520303>
- McEwen, A. S., Eliason, E. M., Bergstrom, J. W., Bridges, N. T., Hansen, C. J., Delamere, W. A., et al. (2007). Mars reconnaissance orbiter's high resolution imaging science experiment (HiRISE). *Journal of Geophysical Research*, 112(E5), E05S02. <https://doi.org/10.1029/2005JE002605>
- McLennan, S. M., Bell, III, J., Calvin, W., Christensen, P., Clark, B., de Souza, P., et al. (2005). Provenance and diagenesis of the evaporite-bearing Burns formation, Meridiani Planum, Mars. *Earth and Planetary Science Letters*, 240(1), 95–121. <https://doi.org/10.1016/j.epsl.2005.09.041>
- McMahon, S., Bosak, T., Grotzinger, J. P., Milliken, R. E., Summons, R. E., Daye, M., et al. (2018). A field guide to finding fossils on Mars. *Journal of Geophysical Research: Planets*, 123(5), 1012–1040. <https://doi.org/10.1029/2017JE005478>
- Merényi, E., Singer, R. B., & Miller, J. S. (1996). Mapping of spectral variations on the surface of Mars from high spectral resolution telescopic images. *Icarus*, 124(1), 280–295. <https://doi.org/10.1006/icar.1996.0204>

- Metcalfe, R., Rochelle, C. A., Savage, D., & Higgs, J. W. (1994). Fluid-rock interactions during continental red bed diagenesis: Implications for theoretical models of mineralization in sedimentary basins. *Geological Society Special Publication*, 78(1), 301–324. <https://doi.org/10.1144/GSL.SP.1994.078.01.2>
- Meyer, M. A., Kminek, G., Beaty, D. W., Carrier, B. L., Haltigin, T., Hays, L. E., et al. (2022). Final Report of the Mars Sample Return Science Planning Group 2 (MSPG2). *Astrobiology*, 22(S1), S5–S26. <https://doi.org/10.1089/ast.2021.0121>
- Minitti, M. E., Kennedy, M., Edgett, K. S., Beegle, L. W., Asher, S., Abbey, W. J., et al. (2019). The Mars 2020 WATSON Imaging Subsystem of the SHERLOC Investigation and anticipated early results. *Journal of Geophysical Research: Planets*, 124(2), 528–584. <https://doi.org/10.1029/2018JE005774>
- Morris, R. V., Klingelhöfer, G., Schröder, C., Rodionov, D. S., Yen, A., Ming, D. W., et al. (2006). Mössbauer mineralogy of rock, soil, and dust at Meridiani Planum, Mars: Opportunity's journey across sulfate-rich outcrop, basaltic sand and dust, and hematite lag deposits. *Journal of Geophysical Research*, 111(E12), E12S15. <https://doi.org/10.1029/2006JE002791>
- Nachon, M., López-Reyes, G., Meslin, P. Y., Ollila, A. M., Mandon, L., Clavé, E., et al. (2023). Light-toned veins and material in Jezero Crater, Mars, as seen in-situ via NASA Perseverance Rover (Mars 2020 mission): Stratigraphic distribution and compositional results from the SuperCam instrument. In *Lunar and Planetary Science Conference* (Vol. 2673).
- Novoselov, A. A., Roberto, C., & Filho, D. S. (2015). Potassium metasomatism of Precambrian paleosols. *Precambrian Research*, 262, 67–83. <https://doi.org/10.1016/j.precamres.2015.02.024>
- Paige, D. A., Hamran, S. E., Amundsen, H. E. F., Berger, T., Russell, P., Kakaria, R., et al. (2024). Ground penetrating radar observations of the contact between the western delta and the crater floor of Jezero crater, Mars. *Science Advances*, 10(4), eadi8339. <https://doi.org/10.1126/sciadv.adi8339>
- Parry, W. T., Chan, M. A., & Beitler, B. (2004). Chemical bleaching indicates episodes of fluid flow in deformation bands in sandstone. *American Association of Petroleum Geologists Bulletin*, 88(2), 175–191. <https://doi.org/10.1306/09090303034>
- Phua, Y. Y., Ehlmann, B. L., Siljeström, S., Czaja, A. D., Beck, P., Connell, S., et al. (2024). Characterizing hydrated sulfates and altered phases in Jezero Crater fan and floor geologic units with SHERLOC on Mars 2020. *Journal of Geophysical Research: Planets*, 129(7), e2023JE008251. <https://doi.org/10.1029/2023JE008251>
- PiPujol, M. D., & Buurman, P. (1994). The distinction between ground-water gley and surface-water gley phenomena in Tertiary paleosols of the Ebro basin, NE Spain. *Palaeogeography, Palaeoclimatology, Palaeoecology*, 110(1–2), 103–113. [https://doi.org/10.1016/0031-0182\(94\)90112-0](https://doi.org/10.1016/0031-0182(94)90112-0)
- Pontefract, A., Zhu, T. F., Walker, V. K., Hepburn, H., Lui, C., Zuber, M. T., et al. (2017). Microbial diversity in a hypersaline sulfate lake: A terrestrial analog of ancient Mars. *Frontiers in Microbiology*, 8, 1819. <https://doi.org/10.3389/fmicb.2017.01819>
- Potter-McIntyre, S. L., Chan, M. A., & McPherson, B. J. (2014). Concretion formation in volcanoclastic host rocks: Evaluating the role of organics, mineralogy, and geochemistry on early diagenesis. *Journal of Sedimentary Research*, 84(10), 875–892. <https://doi.org/10.2110/jsr.2014.58>
- Quantin-Nataf, C., Alwmark, S., Calef, F. J., Lasue, J., Kinch, K., Stack, K. M., et al. (2023). The complex exhumation history of Jezero crater floor unit and its implication for Mars sample return. *Journal of Geophysical Research: Planets*, 128(6), e2022JE007628. <https://doi.org/10.1029/2022JE007628>
- Rampe, E. B., Blake, D., Bristow, T., Ming, D., Vaniman, D., Morris, R., et al. (2020). Mineralogy and geochemistry of sedimentary rocks and eolian sediments in Gale crater, Mars: A review after six Earth years of exploration with Curiosity. *Geochemistry*, 80(2), 125605. <https://doi.org/10.1016/j.chemer.2020.125605>
- Rapin, W., Dromart, G., Clark, B. C., Schieber, J., Kite, E. S., Kah, L. C., et al. (2023). Sustained wet–dry cycling on early Mars. *Nature*, 620(7973), 299–302. <https://doi.org/10.1038/s41586-023-06220-3>
- Rapin, W., Ehlmann, B. L., Dromart, G., Schieber, J., Thomas, N. H., Fischer, W. W., et al. (2019). An interval of high salinity in ancient Gale crater lake on Mars. *Nature Geoscience*, 12(11), 889–895. <https://doi.org/10.1038/s41561-019-0458-8>
- Retallack, G. J. (1991). Untangling the effects of burial alteration and ancient soil formation. *Annual Review of Earth and Planetary Sciences*, 19(1), 183–206. <https://doi.org/10.1146/annurev.earth.19.050191.001151>
- Rice, M. S., Johnson, J. R., Million, C. C., St. Clair, M., Horgan, B. N., Vaughan, A., et al. (2022). Mastcam-Z multispectral database from the Perseverance rover's traverse in the Jezero crater floor, Mars (sols 0–380) [Dataset]. *WWU Geology Faculty Publications*. <https://doi.org/10.25710/bhyk-kc32>
- Rice, M. S., Johnson, J. R., Million, C. C., St. Clair, M., Horgan, B. N., Vaughan, A., et al. (2023). Spectral variability of rocks and soils on the Jezero crater floor: A summary of multispectral observations from Perseverance's Mastcam-Z Instrument. *Journal of Geophysical Research: Planets*, 128(10), e2022JE007548. <https://doi.org/10.1029/2022JE007548>
- Royer, C., Poulet, F., Wiens, R. C., Mandon, L., Fouchet, T., & Clave, E. (2023). Jezero Delta mineralogical diversity revealed by SuperCam infrared spectral modeling. In *Lunar and Planetary Science Conference* (Vol. 2806).
- Rudolph, A., Horgan, B., Johnson, J., Bennett, K., Haber, J., Bell, J., et al. (2022). The distribution of clay minerals and their impact on diagenesis in Glen Torridon, Gale crater, Mars. *Journal of Geophysical Research: Planets*, 127(10), e2021JE007098. <https://doi.org/10.1029/2021JE007098>
- Song, B., Zhang, K., Zhang, L., Ji, J., Hong, H., Wei, Y., et al. (2018). Qaidam Basin paleosols reflect climate and weathering intensity on the northeastern Tibetan Plateau during the Early Eocene Climatic Optimum. *Palaeogeography, Palaeoclimatology, Palaeoecology*, 512, 6–22. <https://doi.org/10.1016/j.palaeo.2018.03.027>
- Spinola, D. N., de Castro Portes, R., Srivastava, P., Torrent, J., Barrón, V., & Kühn, P. (2018). Diagenetic reddening of Early Eocene paleosols on King George Island, Antarctica. *Geoderma*, 315, 149–159. <https://doi.org/10.1016/j.geoderma.2017.11.010>
- Squyres, S. W., Grotzinger, J. P., Arvidson, R. E., Bell, III, J. F., Calvin, W., Christensen, P. R., et al. (2004). In situ evidence for ancient aqueous environment at Meridiani Planum, Mars. *Science*, 306(5702), 1709–1715.
- Stack, K. M., Grotzinger, J. P., Kah, L. C., Schmidt, M. E., Mangold, N., Edgett, K. S., et al. (2014). Diagenetic origin of nodules in the Sheepbed member, Yellowknife Bay formation, Gale crater, Mars. *Journal of Geophysical Research: Planets*, 119(7), 1637–1664. <https://doi.org/10.1002/2014JE004617>
- Stack, K. M., Ives, L. R. W., Gupta, S., Lamb, M. P., Tebolt, M., Caravaca, G., et al. (2024). Sedimentology and stratigraphy of the Shenandoah formation, western fan, Jezero crater, Mars. *Journal of Geophysical Research: Planets*, 129(2), e2023JE008187. <https://doi.org/10.1029/2023JE008187>
- Stack, K. M., Williams, N. R., Calef, III, F., Sun, V. Z., Williford, K. H., Farley, K. A., et al. (2020). Photogeologic map of the perseverance rover field site in Jezero Crater constructed by the Mars 2020 Science Team. *Space Science Reviews*, 216(8), 127. <https://doi.org/10.1007/s11214-020-00739-x>

- St. Clair, M., Million, C., & Rice, M. (2022). Marslab software suite [Software]. *Zenodo*. Retrieved from <https://zenodo.org/badge/latestdoi/498892781>
- Sun, V. Z., Hand, K. P., Stack, K. M., Farley, K. A., Simon, J. I., Newman, C., et al. (2023). Overview and results from the Mars 2020 Perseverance rover's first science campaign on the Jezero crater floor. *Journal of Geophysical Research: Planets*, 128(6), e2022JE007613. <https://doi.org/10.1029/2022JE007613>
- Sun, V. Z., Stack, K. M., Kah, L. C., Thompson, L., Fischer, W., Williams, A. J., et al. (2019). Late-stage diagenetic concretions in the Murray formation, Gale crater, Mars. *Icarus*, 321, 866–890. <https://doi.org/10.1016/j.icarus.2018.12.030>
- Tate, C., Hayes, A. G., Kanine, O., Gupta, S., Caravaca, G., & Paar, G. (2023). Stratigraphic reconstruction and analysis of the delta remnant Kodiac in Jezero crater, Mars. In *Lunar and Planetary Science Conference* (Vol. 2806).
- Thorpe, M. T., Bristow, T. F., Rampe, E. B., Tosca, N. J., Grotzinger, J. P., Bennett, K. A., et al. (2022). Mars Science Laboratory CheMin data from the Glen Torridon region and the significance of lake-groundwater interactions in interpreting mineralogy and sedimentary history. *Journal of Geophysical Research: Planets*, 127(11), e2021JE007099. <https://doi.org/10.1029/2021JE007099>
- Turner, S. M. R., Schwenzer, S. P., Bridges, J. C., Rampe, E. B., Bedford, C. C., Achilles, C. N., et al. (2021). Early diagenesis at and below Vera Rubin ridge, Gale crater, Mars. *Meteoritics & Planetary Sciences*, 56(10), 1905–1932. <https://doi.org/10.1111/maps.13748>
- Vaughan, A., Minitti, M. E., Cardarelli, E. L., Johnson, J. R., Kah, L. C., Pilleri, P., et al. (2023). Regolith of the crater floor units, Jezero crater, Mars: Textures, composition, and implications for provenance. *Journal of Geophysical Research: Planets*, 128(3), e2022JE007437. <https://doi.org/10.1029/2022JE007437>
- Watanabe, Y., Martin, J. E., & Ohmoto, H. (2000). Geochemical evidence for terrestrial ecosystems 2.6 billion years ago. *Nature*, 408(6812), 574–578. <https://doi.org/10.1038/35046052>
- Watanabe, Y., Stewart, B. W., & Ohmoto, H. (2004). Organic- and carbonate-rich soil formation ~2.6 billion years ago at Schagen, East Transvaal district, South Africa. *Geochimica et Cosmochimica Acta*, 68(9), 2129–2151. <https://doi.org/10.1016/j.gca.2003.10.036>
- Wiens, R. C., Maurice, S., Robinson, S. H., Nelson, A. E., Cais, P., Bernardi, P., et al. (2021). The SuperCam instrument suite on the NASA Mars 2020 rover: Body unit and combined system tests. *Space Science Reviews*, 217(1), 4. <https://doi.org/10.1007/s11214-020-00777-5>
- Wiens, R. C., Udry, A., Beyssac, O., Quantin-Nataf, C., Mangold, N., Cousin, A., et al. (2022). Compositionally and density stratified igneous terrain in Jezero crater, Mars. *Science Advances*, 8(34), eabo3399. <https://doi.org/10.1126/sciadv.abo3399>

References From the Supporting Information

- Cardarelli, E. L., Bargar, J. R., Francis, C. A., & Francis, C. A. (2020). Diverse Thaumarchaeota dominate subsurface ammonia-oxidizing communities in semi-arid floodplains in the Western United States. *Environmental Microbiology*, 80(4), 778–792. <https://doi.org/10.1007/s00248-020-01534-5>
- Haber, J. T., Horgan, B. H. N., Potter-McIntyre, S. L., Broz, A. P., & Smith, R. J. (2023). Evidence of increased surface exposure and diagenetic alteration in evaporitic environments on Earth and Mars. In *Lunar and Planetary Science Conference* (pp. 4–5).
- Noël, V., Boye, K., Kukkadapu, R. K., Bone, S., Lezama, J. S., Cardarelli, E., et al. (2017). Understanding controls on redox processes in floodplain sediments of the Upper Colorado River Basin. *Science of the Total Environment*, 603–604, 663–675. <https://doi.org/10.1016/j.scitotenv.2017.01.109>